Ts66Yah, a refined Ts65Dn DS mouse model, unravels genetic interaction between regions homologous to Human chromosome 21 and the Scaf8-Pde10a genetic interval.

Arnaud Duchon[1], Maria del Mar Muñiz Moreno[1], Claire Chevalier[1], Valérie Nalesso[1], Philippe Andre[2], Marta Fructuoso-Castellar[3,4,5,6], Mary Mondino[7], Chrystelle Po[7], Vincent Noblet[7], Marie Christine Birling[2], Marie-Claude Potier[3,4,5,6] and Yann Herault[1,2,*]

[1] Université de Strasbourg, CNRS, INSERM, Institut de Génétique et de Biologie Moléculaire et Cellulaire (IGBMC), department of translational medicine and neurogenetics 1 rue Laurent Fries, 67404 Illkirch Graffenstaden, France
[2] Université de Strasbourg, CNRS, INSERM, CELPHEDIA, PHENOMIN-Institut Clinique de la Souris (ICS), 1 rue Laurent Fries, 67404 Illkirch Graffenstaden, France
[3] Paris Brain Institute ICM, Hôpital de la Pitié-Salpêtrière, Paris, France.
[4] Institut National de la Santé et de la Recherche Médicale, U1127, Hôpital de la Pitié-Salpêtrière, Paris, France.
[5] Centre National de la Recherche Scientifique, UMR7225, Hôpital de la Pitié-Salpêtrière, Paris, France.
[6] Sorbonne Université, Hôpital de la Pitié-Salpêtrière, Paris, France.
[7] Université de Strasbourg, CNRS UMR 7357, ICube, FMTS, 67000 Strasbourg, France
*Corresponding author:
Tel.: +33 3 88 65 5657 (Assistant) or 5715 (Direct) Email: herault@igbmc.fr

ABSTRACT

Down syndrome is the consequence of trisomy of human chromosome 21 (Hsa21). The understanding of phenotype-genotype relationships, the identification of driver genes and various proof-of-concepts for therapeutic improvement have benefited from the development of mouse models. The premier model, named Ts(17^{16})65Dn/J (Ts65Dn), corresponds to an additional minichromosome with the *Mir155* to *Zbtb21* region of mouse chromosome 16 (Mmu16), homologous to Hsa21, encompassing around 90 genes, fused to the centromeric part of mouse chromosome 17 (Mmu17). The Ts65Dn line displayed several phenotypes related to the human features found in people with DS. The detailed analysis of the Ts65Dn minichromosome unraveled the presence of 46 trisomic genes from the centromeric region of Mmu17, from *Pisd-ps2/Scaf8* to *Pde10a,* not related to Hsa21. Here, we report the investigation of a new model, Ts66Yah, generated by CrispR/Cas9 to remove the genomic region unrelated to Hsa21 on the minichromosome. Not surprisingly, the sole presence of 3 copies of the *Mir155-Zbtb21* interval in Ts66Yah induces DS related features. However, the loss of certain phenotypes related to increased activity, spatial learning and specific molecular signatures suggest strong genetic interactions between the *Mir155-Zbtb21* and the *Scaf8-Pde10a* interval. Thus, Ts66Yah mice have a stronger construct and face validity for mimicking specific consequences of DS genetic overdosage, certainly more translatable to humans and with potential better proof-of-concept studies for therapeutics. Furthermore, this report is the first to demonstrate genetic interactions between triplicated regions homologous to Hsa21 and others unrelated to Hsa21.

48 **INTRODUCTION**

49 Advanced knowledge of the pathophysiology of Down syndrome (DS), commonly known as
50 trisomy 21, has been acquired from mouse models. Animal research has allowed the
51 identification of several major driver genes linked to the clinical features found in people with
52 DS, such as DYRK1A and CBS, and made possible the pre-clinical validation of therapies with
53 several drug candidates (DUCHON and HERAULT 2016; HERAULT *et al.* 2017; NAKANO-KOBAYASHI *et*
54 *al.* 2017; FAUNDEZ *et al.* 2018; NEUMANN *et al.* 2018; NGUYEN *et al.* 2018; MARECHAL *et al.* 2019).
55 Over the last decades, even more complex mouse models have been generated carrying one
56 human chromosome 21 almost complete (O'DOHERTY *et al.* 2005; KAZUKI *et al.* 2020), and
57 various segmental duplications of regions homologous to human chromosome 21 (Hsa21; Hsa
58 for *Homo Sapiens*) making it possible to dissect genotype-phenotype relationships in DS
59 (HERAULT *et al.* 2017; DUCHON *et al.* 2021).

60 These studies were pioneered and strongly driven by the use of the Ts(17^{16})65Dn/J (Ts65Dn)
61 mouse line. This model developed by Muriel Davidson and Roger Reeves (DAVISSON *et al.* 1990;
62 DAVISSON *et al.* 1993; REEVES *et al.* 1995), is commercially available and is widely used for DS
63 research, with more than 500 publications found in the PUBMED database (April 2022).
64 Originally, the Ts(17^{16})65Dn/J line was generated by the irradiation of DBA/2J males, then
65 crossed with C57BL/6J females, with the progeny being checked for chromosomal
66 abnormalities (Davisson et al., 1990; Davisson et al., 1993). Translocations for murine
67 chromosome 16 (Mmu16 for *Mus musculus*) homologous to Hsa21 were then mated with the
68 C57BL/6J x C3H/HeJ F1 hybrid line. The genetic background of B6C3HF1 was selected to obtain
69 large litters and maintain higher transmission of the translocated minichromosome
70 Ts(17^{16})65Dn/J, encompassing 90 protein coding genes (PGCs) from *Mir155* to *Zbtb21,* linked
71 to the centromeric part of the Mmu17 chromosome which contains a region non-homologous

72 to Hsa21, from *Pisd-ps2* to *Pde10a* (for approximately 46 PGCs; (MUÑIZ MORENO *et al.* 2020)).
73 The region *Pisd-ps2 to Pde10a* is homologous to the region between *SCA8* and *PDE10A,* found
74 on human chromosome 6. Due to this rearrangement, the genetic validity of the model has
75 been a topic of debate for quite some time. On the one hand, the presence of a
76 supernumerary freely segregating chromosome may contribute to producing additional
77 phenotypes as compared to models with intrachromosomic duplications (GOODLIFFE *et al.*
78 2016; OLMOS-SERRANO *et al.* 2016); on the other hand, the presence of 60 genes non-
79 homologous to Hsa21 may have a phenotypic impact not related to DS, and too often
80 neglected in various studies. Somehow, the effect of this additional triplicated segment has
81 been set aside and its contribution to Ts65Dn phenotypes remains undetermined.
82 To solve this dilemma and have a model closer to DS, we developed a new line named
83 Ts66Yah, derived from the Ts65Dn lineage but no longer carrying the duplicated centromeric
84 part of Mmu17. Here, we report its first phenotypic and molecular characterization. The
85 Ts66Yah mouse model was generated using CrispR/Cas9 technology in vivo to remove the
86 segment of DNA corresponding to the centromeric Mmu17 located on the Ts65Dn
87 minichromosome. Using comparative genomic hybridization array (a-CGH), we verified that
88 the CrispR/Cas9 deletion completely removed the segment. Then, we performed the
89 phenotypic characterization of the new Ts66Yah line using a classical battery of behavioral
90 tests in young adult mice and compared to Ts65Dn mice produced in parallel. Cohorts of adult
91 trisomic and control littermates were tested for nesting activity, circadian activity, exploration
92 of a novel environment in the open field (noted as OF), spontaneous alternation in the Y maze
93 (noted as Y-maze), object recognition (noted as OR), spatial memory in the Morris water maze
94 test (noted as MWM), associative memory in fear conditioning (noted as FC). Most of the tests
95 with significant results were replicated in a second laboratory to check their robustness. We

96 also performed morphometric analysis based on MRI and µCT scans, respectively for the brain
97 and the skull, and a high throughput gene expression analysis based on population-based
98 transcriptome analysis to identify the genetic and functional alterations in the hippocampus
99 and entorhinal cortex of Ts66Yah and make the comparison with the Ts65Dn model.
100
101 **RESULTS**
102 **Structure of the *Scaf8-Pde10a* proximal region of mouse chromosome 17**
103 Before creating the Ts66Yah model we looked at the *Scaf8-Pde10a* region. We found it quite
104 rearranged in several mouse lines according to the mouse genome informatics database. In
105 particular we closely investigated the corresponding segments in the DBA/2J line used to
106 generate the first Ts65Dn chromosome, and also in C57BL/6J and C3H/HeJ (as a proxy) of the
107 mouse lines used to breed the Ts65Dn mouse carriers. Overall, the region was globally
108 conserved in its organization but several loci were affected (Fig. S1A). More precisely, the *Snx9*
109 locus was different in size in the 3 models, and more perturbed in C3H/HeJ. Remarkably, the
110 genetic interval encompassing *Tulp4, Tmem181a and Sytl3* were not found in the DBA/2J
111 genome and other loci for *Rpsh3* and *Rnaset2* were duplicated differently in the 3 genetic
112 backgrounds (Fig. S1B). Interestingly, the region is well preserved in humans on Chromosome
113 6 with an organization similar to that of C57BL/6J, except for large inversions near the *Pde10a*
114 and *Rps6ka2-Rnaset2* genes that occurred during evolution.
115
116 **Creation, validation, and transmission of the new Ts66Yah minichromosome**
117 Thus, we decided to remove the centromeric segment of Mmu17 located on the Ts65Dn
118 minichromosome using the CrispR/Cas9 technique. Embryos obtained from in vitro
119 fertilization, taking sperm from selected fertile Ts65Dn male and wild-type F1B6C3B oocytes,

120 were injected with CrispR/Cas9 and the pairs of selected gRNAs based on the CRISPOR score
121 (CONCORDET and HAEUSSLER 2018)(Fig. 1A). One founder carrying the recombined
122 minichromosome, with the deletion of the centromeric part of Mmu17, was selected in the
123 progeny and crossed with C57BL/6NCrl females. Two offspring, one male and one female,
124 were used to start the new colony. The extent of the deletion was characterized by Sanger
125 sequencing of the PCR fragment encompassing the region deleted from the centromeric part
126 on Mmu17 to Mmu16 (Fig. 1B-C), leaving a piece of Mmu16 encompassing the *Mir155* to the
127 end of the telomeric Mmu16 (about 13,856,661 bp). We characterized the new breakpoint
128 between the genomic base number 3,071,436 on Mmu17 and the base 84,354,894 on Mmu16
129 (UCSC Genome Browser on Mouse Dec. 2011 (GRCm38/mm10) Assembly).
130 We confirmed the presence of an independent chromosome on metaphase spreads where we
131 could clearly see the 40 mouse chromosomes plus one minichromosome in Ts66Yah
132 embryonic fibroblasts isolated from 14.5 days post coitum (dpc) mutant embryos (Fig. 1D).
133 We also performed a-CGH to check the copy number of the Mmu16 and Mmu17
134 chromosomes both in the Ts66Yah and Ts65Dn models (Fig. 1E). We were able to confirm that
135 the Ts66Yah model indeed lacks the increase in gene dosage for the telomeric part of the
136 Mmu17 region from *Pisd-ps2* to *Pde10a* seen in the Ts65Dn model (Fig. 1E-F), while the copy
137 number of the region located on Mmu16 homologous to Hsa21 increased. Moreover, we
138 checked that the change in the Mmu16 copy number in the Ts66Yah mice was located
139 upstream of *Mrpl39* (DUCHON *et al.* 2011b), as expected, between two probes targeting the
140 Mmu16 genetic interval 84,325,686-84,356,080 from the mouse genome assembly
141 GRCm38/mm10.
142 We also checked the genetic transmission of the minichromosome. After establishing the line,
143 we obtained a good transmission rate of about 50% per litter (Table 1). Then, the transmission

144 rate began to decrease with the number of backcrosses on a pure genetic background
145 (C57BL/6J, up to N4). We thus decided to maintain the mixed genetic background used for the
146 Ts65Dn mice, with the sighted C3H (C3B) males crossed with B6J females, namely B6C3B, that
147 we commonly use in our laboratory. Currently, we have a stable ratio of transmission from
148 both male and female germlines (Table 1), although not all the Ts66Yah males are fertile. We
149 hypothesize that the increased fertility of Ts66Yah was a consequence of the selection of
150 fertile Ts65Dn males when generating the model. To test this, we performed a sperm analysis
151 to evaluate the quality of the sperm by looking at different parameters such as the
152 concentration of spermatozoids, their motility, their velocity and progressivity, for both
153 Ts66Yah and Ts65Dn lines (Fig. S2). As expected, the Ts65Dn mice showed poorer performance
154 than wild-type littermates for all the sperm parameters analyzed. Similar differences were also
155 observed in the Ts66Yah male sperm, with lower quality than the wild-type (wt) littermates.
156 Nonetheless, we were able to isolate 23 fertile males out of the 39 identified in the Ts66Yah
157 line which is in the range of the published results for Ts65Dn (MOORE *et al.* 2010).

158 **The Ts66Yah mice displayed lower locomotor activity compared to the Ts65Dn mice in many**
159 **tests**

160 To study the behavioral phenotypes of both models under the same environmental
161 conditions, we produced separate cohorts for the two DS models from crosses of wt B6C3B
162 males with Ts66Yah or Ts65Dn females. Then, we challenged the Ts66Yah, Ts65Dn and wild-
163 type littermate animals to a battery of behavioral tests.

164 First, we assessed their adaptation to a novel environment and exploration activity in a
165 brightly illuminated (120 Lux) square open field. Under this strong light, the animal can choose
166 to explore the center of the open field and be more exposed, or to stay in a safer position at
167 the periphery along the walls of the open field. The Ts66Yah mutant mice showed the same

168 pattern of exploration as their wild-type littermates, with no significant differences between
169 the two groups for either the distance travelled or the number of rears (Fig. S3A). In contrast,
170 the Ts65Dn mice travelled further, notably more in the peripheral zone, and performed fewer
171 rears in the central zone compared to their wild-type littermates. These results therefore
172 indicate that only the Ts65Dn mutants, but not the Ts66Yah, presented an increase in anxiety-
173 like behavior, as emphasized by the reduced activity in the center of the arena, and the
174 increased activity in the peripheral zone of the open field.
175 We then wondered if the circadian activity of the mutant animals was altered, as reported
176 previously for the Ts65Dn model (RUBY *et al.* 2010). We therefore tested the activity of the
177 mice for 46 hours (2 nights). Ts66Yah and Ts65Dn mutants exhibited a similar pattern of
178 circadian activity compared to their control littermates (Fig. S3B). However, we observed that
179 the distance travelled by the Ts65Dn mutants was increased in the light and dark phases
180 compared to the control mice, whereas the activity level of the Ts66Yah mice was comparable
181 to the controls. This result was confirmed by the number of rears, which was also increased in
182 the Ts65Dn line, even in the habituation phase. Similar increases in activity were observed in
183 the number of Y Maze arm entries (Fig. S3C). Thus, the hyperactivity phenotype detected in
184 the Ts65Dn mutants in several paradigms was absent in the Ts66Yah.

185 **Robust cognitive deficits in the Ts66Yah mouse models**

186 Several learning and memory deficits have been described in the Ts65Dn mouse line with
187 unanimity by different teams, and are considered as robust and reproducible phenotypes
188 (REEVES *et al.* 1995; MARTINEZ-CUE *et al.* 2002; FERNANDEZ *et al.* 2007; GARCÍA-CERRO *et al.* 2017;
189 AZIZ *et al.* 2018; DUCHON *et al.* 2021). Thus, we tested how much those robust phenotypes, so
190 widely reproduced, were present in the Ts66Yah individuals.

191 First, we started to analyze alterations linked to the normal innate behavior of rodents with
192 the nest building task, which is sensitive to hippocampal lesions and is an ancillary parameter
193 assessed to predict cognitive defects (HELLER *et al.* 2014). The organization of the nest was
194 scored after one night with a scale from 0, equivalent to the absence of a nest, to 5 when a
195 full dome is raised. For both lines, most control disomic mice built a nest with a dome (score
196 higher than 3; Fig. 2A) nevertheless the nesting score was lower for both trisomic lines
197 compared to the control littermates. Intriguingly, 9 out of 25 Ts66Yah males built a nest with
198 a score above 3 while only 2 males out of 12 reach this stage in the Ts65Dn. Further
199 investigation would be needed to confirm this observation.
200 Then, we assessed spatial working memory by placing the mice in a Y-maze and left them to
201 freely explore the three arms. The total number of entries to any arm was scored as an index
202 of locomotor activity. In the Ts66Yah mouse line, the percentage of alternation of the mutant
203 mice was significantly different from 50% (chance level) but no strong difference was observed
204 between trisomic and control individuals. On the contrary, there was a strong difference for
205 the Ts65Dn mutants who showed a lower percentage of spontaneous alternation than their
206 control littermates, with a percentage of alteration for the mutant group significantly different
207 from 50% (Fig. 2B).
208 Afterwards, we evaluated the episodic non-spatial recognition memory using the novel object
209 recognition (NOR) paradigm with a retention time of 24h. During the acquisition session
210 (presenting two identical objects), there was a difference in the exploration time between
211 both Ts65Dn and Ts66Yah mutant animals versus their respective control groups (Fig S4A).
212 Indeed, both DS model mice spent more time to explore the objects. During the test session,
213 24 h after the acquisition session, when one of the two familiar objects was replaced by a new
214 one, both DS mice models explored both objects at the same rate (the discrimination index

215 was close to 50%) and did not show any preference for the novel object contrary to the control
216 mice (Fig. 2C). The Y-maze and object recognition phenotypes were reproduced in an
217 independent group of male and female mice mice bred and tested in a second laboratory,
218 without any sex effect.(Fig. S5).
219 In the next step, we focused on the spatial reference memory in the Morris water maze
220 (MWM) task. Mice must learn how to escape from a circular pool of opaque water by localizing
221 a hidden platform (PF), set at a single fixed location, using distal spatial cues. Three different
222 sessions were organized according to the diagram shown in Fig. 3A. First, a standard learning
223 phase session where a hidden platform is presented was performed, followed by a reversal
224 session to detect memory flexibility. Both sessions ended with a probe test. Finally, a visible
225 session was performed to assess the general capacity of the mice to perform the test and
226 asses any visual or physical impairments. We measured the velocity, thigmotaxis and time
227 spent by each individual to reach the platform. For the Ts66Yah line (Fig. 3B-I), there was no
228 significant difference between the mutant and control group for thigmotaxis and swimming
229 speed; however, the Ts66Yah mutants took longer to reach the platform during the sessions,
230 indicating poorer performance than the control group. Apart from this, Ts66Yah mice learned
231 the PF location at the last block of the trial with half the latency as over the first block of the
232 trial. The same profile was observed in the reversal phase. The retention of place location was
233 assessed during a single probe trial (PT) with no platform available, 24h after the last training
234 session. In this probe test, all the mice remembered where the platform was located after the
235 two learning sessions (learning and reversal phase). As expected, the Ts65Dn mutants (Fig. 3J-
236 Q) presented an increased level of thigmotaxis compared to the controls and an increased
237 latency, indicating that the mutants had difficulties in learning the PF location. This conclusion
238 was supported by the analysis of the reversal phase data. In addition, the Ts65Dn mutants did

239 not present any preference for the target quadrant, with a level of time exploration close to
240 25% for both the learning and reversal phases. Efficacy depends on swimming strategies to
241 search for the PF. Thus, we analyzed the strategies to search for the PF undertaken by each
242 individual along the test phase. Only the Ts65Dn mice showed a low and constant high level
243 of non-spatial navigation while the level of spatial strategy increased both in the 2n mice and
244 in the Ts66Yah animals during learning in the sessions of both the initial learning and reversal
245 phase but not in Ts65Dn mice (Fig. S4B). In the visible session (Fig. S4B), the Ts66Yah latency
246 to reach the PF was longer that of the control mice, with a wider distribution. However, the
247 mean of the latency was definitely less than the mean of the latency in the last session of the
248 reversal phase. This indicates that the mice did not have any deficit that could have prevented
249 them from learning and passing the test. Overall, our results confirmed a severe impaired
250 spatial learning in Ts65Dn mice but not in the Ts66Yah mice.
251 Finally, both mutant lines were tested for contextual associative memory deficits in the
252 Pavlovian fear conditioning test. To induce fear responses, the mice were placed in a “fear
253 context”, a context box where they were subjected to an electric shock. When the animals
254 were re-subjected to the shock 24 h later in the same “fear context”, the level of freezing in
255 all groups was increased compared to the habituation session, indicating that all groups
256 developed a behavioral fear response during the training session (Fig. S4C). The Ts65Dn
257 mutants presented a lower level of responses than the control group, especially at the end of
258 the context session (the last 2 minutes of the session named CONT3). On the contrary, the
259 Ts66Yah mutants did not show any difference in freezing time compared to the control group.
260 Thus, we concluded that the hyperactivity of Ts65Dn mutants interfered with this test: the
261 Ts65Dn mutants would not be subject to a memory failure but instead could not stop moving
262 during a session lasting 2min.

263 **Identification of discriminating phenotypic variables between Ts66Yah and Ts65Dn**

264 Considering the differences observed in several phenotypic behavioral variables (Table S1) we
265 wanted to assess the importance of each variable for the genotype-based classification using
266 both the Elastic-Net Regularized Generalized Linear Model (GLM-Net) and random forests (RF)
267 with GDAPHEN (see Materials and Methods). First, we found that several of all the variables
268 considered for the analysis (Table S2) were highly correlated (more than 86% correlation) and
269 thus were removed from the respective downstream analysis for both Ts65Dn and Ts66Yah
270 with their respective wild-type controls (Table S3). The statistical classifiers GLM-Net and RF
271 identified several variables that discriminated the trisomic from the control individual in each
272 model separately (Fig. 4). Using both classifiers, the three most important variables to
273 discriminate Ts66Yah versus wild-type individuals were the "sperm concentration", the
274 "sperm:progressive", and the "percentage of time spent in the target quadrant in the 1st probe
275 test" (MWM:PTRev_TQ; GLM-NET; table S5) with the "nesting score" (RF; table S5; Fig. 4A).
276 In addition, the wt and trisomic individuals were easily separated in principal component
277 analysis (PCA; Fig. 4B) with 67% of the variance explained with the 3 first dimensions (Fig. 4C).
278 To discriminate Ts65Dn versus wild-type individuals, the situation was different with both
279 classifiers (Fig. 4D, table S5). The most important variables were also the ""FC:Precue1 (GLM-
280 Net) and the "sperm concentration" (RF), then the "FC:Cont3" for both and in third position
281 "MWM:PT1_TQ" (GLM-Net) with the "FC:Precue1" for RF (table S5; Fig. 4D). About 59% of the
282 variance was explained with the 3 first dimensions of the PCA to separate Ts65Dn and wt
283 individuals (Fig. 4F). Then we analyzed the discriminating variable combining all the genotypes
284 (Table 2, Fig. S6), and we found more behavioral variables to discriminate the wt and trisomic
285 individuals. Apart from the first one, "Sperm:Progressive", the next six variables were all
286 derived from behavior tests with "FC:Hab2", "MWM:PTRev_TQ", "NOR:Test_NO",

287 “YM:Spont_Alter”, “CA:Rears:N2”CA:Locomotion:Light”, although the percentage of variance
288 explained was even lower in the 3 first dimensions, with only 46%. The multiple factor analysis
289 (MFA) computed the correlation between the qualitative or quantitative variables grouped by
290 test or ungrouped, and the principal component dimensions. For both DS models, the MFA
291 and the cosine diagrams highlighted almost the same variables as the main contributors to
292 differentiate between Ts65Dn or Ts66Yah and their respective wild-types.

293 **Comparison of morphological alterations in the brain and the skull of Ts66Yah and Ts65Dn**
294 **mice**

295 To detect brain morphological alterations of specific regions in the two DS models, we
296 conducted an MRI study. We did not observe statistically significant changes for the whole
297 brain volume. Nevertheless, to be as accurate as possible, we considered the whole brain
298 volume and performed a Z-score standardization (Fig. 5 and S7). Globally, we observed that
299 changes in the morphology of specific brain structures as well as the direction of the changes
300 (increase or decrease of volume) were the same in both DS lines. However, the amplitude of
301 the changes was less severe but statistically significant (Table S1) in Ts66Yah than in Ts65Dn
302 (for example at ventricles, rest of midbrain, fimbria, superior colliculi; Fig. 5 and S7). Principal
303 component analysis (PCA; Fig. S7) comparing mutants with their respective 2n controls for
304 both lines, pointed to a more pronounced difference between the Ts65Dn and their controls
305 than for the Ts66Yah mutants and their controls.

306 People with DS have very specific craniofacial changes which have also been found in Ts65Dn
307 (RICHTSMEIER *et al.* 2000; STARBUCK *et al.* 2014). Thus, we investigated the Ts66Yah, searching
308 for similar craniofacial changes using a landmark based analysis (Table S2, Fig. 5C). PCA
309 computed on Euclidian distance calculated from well-defined landmarks (Fig. 5D) showed that
310 control and trisomic mice were well separated in the Ts66Yah line compared to the Ts65Dn

311 line. The shape differences between groups for skulls and mandibles can be visualized
312 graphically, showing that the deformation was more pronounced in the Y axis than in the X
313 axis (Fig. 5E-F) with the Ts65Dn skull smaller in global size and with more pronounced
314 deformations. Altogether, our brain and skull morphology results demonstrated convergence
315 with DS features in both Ts66Yah and Ts65Dn but with additional changes due to the presence
316 of the trisomy of the *Scaf8-Pde10a* genetic interval in Ts65Dn.
317
318 **The Ts66Yah and Ts65Dn models show a strong tissue specific dysregulation profile in the**
319 **entorhinal cortex and hippocampus with differences in functional alterations**
320 The hippocampus (HIP) and the entorhinal cortex (EC) are two brain regions contributing to
321 novel object recognition (COHEN and STACKMAN 2015; LEAL and YASSA 2015; SCHULTZ *et al.* 2015).
322 Because NOR is affected in both the Ts66Yah and Ts65Dn DS models (This study; (DUCHON *et*
323 *al.* 2021)), we wanted to identify genes and molecular pathways altered in the two models
324 and the two brain regions. Thus, we analyzed the expression profile in both the Ts66Yah and
325 Ts65Dn DS models by focusing on the HIP and EC using RNA-Seq. After normalizing the raw
326 data, we were able to confirm the quality of all the biological replicates as the samples
327 clustered well as a function of their genotype using PCA clustering and the Euclidian distance
328 of all the DEGs identified (Fig. S8 A and B). Then, we performed the differential expression
329 analysis (DEA) and identified 1902 and 2220 DEGs in Ts66Yah HIP and EC respectively, and
330 1836 and 1691 DEGs in the HIP and EC of Ts65Dn (Fig. S8C, table 3). All the DEGs found in both
331 tissues were spread along all the chromosomes although the majority of DEGs were in Mmu16
332 for Ts66Yah and Ts65Dn (Table S8). Interestingly, the misregulation was very specific in the
333 HIP and the EC, with only 417 and 382 genes found misregulated in both regions (HIP∩EC) in
334 Ts66Yah and Ts65Dn respectively. First, regarding the Ts66Yah model, the 417 genes identified

335 commonly dysregulated in both tissues were spread along all the chromosomes and more
336 than 50% were non-coding and pseudogene genomic elements. Of these, 72 had a tissue-
337 specific regulatory sense and more than 60% were non-coding and pseudogenes. Moreover,
338 only 54 genes from Mmu16 were identified as DEGs in both tissues. We found similar results
339 for Ts65Dn with 382 common genes between the regions and 34 from Mmu16. Of these 45
340 have a tissue-specific sense of regulation and more than 70% are non-coding and
341 pseudogenes. Thus, with only around 20% of genes shared between the two brain regions, we
342 concluded that strong tissue specific dysregulation is found in both the Ts65Dn and Ts66Yah
343 models. More globally, we compared the number of DEGs found in both tissues, in Ts65Dn vs
344 Ts66Yah (Fig. 6A). We found 272 common DEGs in the HIP and 282 in the EC (28 are trisomic
345 in Ts65Dn), of these 97 and 105 DEGs follow opposing regulatory senses in both models for
346 the HIP and the EC, respectively (34 are trisomic in Ts65Dn). Those opposing regulated genes
347 could very well be responsible for the differences observed in behavioral analyses.
348 Then, we checked the fold change of trisomic genes along the chromosome regions on Mmu16
349 and 17. We detected a similar fold change for most of the genes located in the Mmu16 region,
350 homologous to human chromosome 21, in the HIP and EC (Fig. S9; Table S8). Out of the 133
351 protein-coding genes (PCG) that are trisomic and located in the segment on Mmu16, 90 and
352 66 showed compensated expression in the Ts66Yah HIP and EC (67 and 49% of the PC trisomic
353 genes), whereas 78 and 100 genes were compensated in the Ts65Dn tissues (58 and 75%
354 respectively; Table 3), thereby supporting previous observations in which approximately half
355 of the trisomic genes are compensated or partially compensated in partial DS models, with a
356 strong effect of the tissue/organ analyzed (AÏT YAHYA-GRAISON *et al.* 2007; DUCHON *et al.* 2021).
357 As expected with the dose effect, the fold changes of the 51 genes (PCG and non-coding),
358 located on the proximal part of Mmu17, were around 1.02+/-0.25 and 1.01+/-0.25 (mean+/-

359 SD) respectively in the Ts66Yah HIP and EC, while they were between 1.54+/-1.22 and 1.63+/-
360 1.2 in the Ts65Dn Hip and EC. Altogether the spearman correlation comparing TEGs from
361 MMu16 in the HIP or EC in both models was low (between 26 to 30%) and was completely loss
362 as expected when looking at TEGs from the centromeric region of the Mmu17 (Fig. S8D).
363 Nevertheless, a few genes from this centromeric interval of Mmu17, trisomic in Ts65Dn but
364 not in Ts66Yah, showed a distinct pattern of expression in the Ts66Yah hippocampi. As
365 expected, 9 genes, *Ezr, Pde10a, Scaf8, Tiam2, Tfb1m, Zdhhc14, Synj2, Serac1* and *Gtf2h5,* were
366 differentially expressed in Ts65Dn but not in Ts66Yah; 2 genes, *Ccr6* and *Tagap,* upregulated
367 in Ts65Dn, were downregulated in Ts66Yah. We verified by qRT-PCR the expression of several
368 genes in the HIP of control and mutant mice. We confirmed the overexpression of *Dyrk1a,*
369 *Sod1* and *Sh3bgr* as expected in both models. We also verified that *Pde10a* and *Ezr* from the
370 Mmu17 region were only upregulated in the Ts65Dn model HIP (Fig. S10) while *Ccr6* was
371 downregulated in Ts66Yah and upregulated in the Ts65Dn HIP. Finally, we also identified genes
372 from Mmu16, syntenic to Hsa21, with an increase of at least 0.5-fold in Ts65Dn compared to
373 the Ts66Yah HIP, with *Kcne1, Kcnj15, Map3k7cl,* and in the EC with *Sh3bgr, Itgb2l, Ripk4* or
374 *Ripply3*, suggesting that the increased dosage of the centromeric Mmu17 genes interfere with
375 the regulation of these genes.
376 On the functional side, we identified 323 and 493 pathways altered in the hippocampi of the
377 Ts66Yah and Ts65Dn models, and 40 and 135 pathways in the EC of both models (Table 3 and
378 S11). This observation suggested a more profound impact in the hippocampi versus the EC,
379 and in the Ts65Dn versus the Ts66Yah conditions (Fig. 6 B). In addition, a milder effect was
380 found in both DS models in the EC samples in comparison with the HIP, and no common
381 pathway was found between Ts65Dn and Ts66Yah in the EC (Fig. 6 A). Next, we identified
382 common alterations per brain region in both DS models; in the HIP, 123 common pathways

383 were altered following the same regulatory sense. Of these, 111 were upregulated involving
384 mainly the immune system, cell adhesion molecules and signaling pathways. However, only
385 10 were downregulated linked to RNA splicing and ncRNA processing (Fig. 6C-D, table S11).
386 The heatmap showing the average number of pathways contributing to meta-pathways with
387 regulatory orientation for the Ts65Dn and Ts66Yah HIP and EC models, supported strong brain
388 region-specific alteration observed in the DEA in both models (Fig. 6B). Interestingly, the
389 samples were clustered by brain regions and not by models. Inside each meta-pathway we
390 identified those that showed a different intensity in the number of pathways altered or in the
391 regulatory sense between both DS models. In addition, the majority of altered pathways in
392 the HIP for both models were upregulated as expected in the light of our results published
393 previously for the Ts65Dn microarray and Dp1Yey models (DUCHON *et al.* 2021). In the EC a
394 lower number of pathways grouped on each meta-pathway were identified compared to the
395 HIP. As such, the HIP showed a higher number of altered pathways and a higher deregulation
396 of "host response", "channels", "metabolism" and "cell structure and organelles".
397 Interestingly the effect was stronger in Ts65Dn compared to Ts66Yah (Fig. 6B). To better
398 understand the region-specific alterations, we compared the HIP and EC meta-pathway maps
399 for each model (Fig. 6C) and between the DS models (Fig. 6D). A few meta-pathways, such as
400 "metabolism", "morphogenesis and development", "channels and location signals" and
401 "enzyme activity", were strongly affected in both DS models, with slightly different levels in
402 the HIP and EC (Fig. 6C). Surprisingly the "cell structure and organelle" were more strongly
403 affected in Ts65Dn than in Ts66Yah, and the "host response" was more affected in both the
404 Ts66Yah and Ts65Dn HIP but only in the EC of Ts65Dn. Moreover, when we compared the HIP
405 and the EC alteration map (Fig. 6D) between Ts66Yah and Ts65Dn, we observed that Ts65Dn
406 showed stronger alterations than Ts66Yah in the "Host and immune response",

407 “Morphogenesis”, “Metabolism and Cell structure” related pathways in the Hippocampi. In
408 addition, the alteration in pathways in the EC was higher in the Ts65Dn model considering the
409 number of total pathways found altered (151 in Ts65Dn, 40 in Ts66Yah) and involved mainly
410 the “Metabolism”, “Enzymes”, “Cell structure”, “Fibers and Cytoskeleton” and “Host and
411 Immune response” meta-pathways.
412 To further understand the nature of the Ts65Dn and Ts66Yah phenotype divergence, we built
413 a regulatory and PPI network, noted RegPPINet, using all the genes identified by gage for
414 Ts65Dn and Ts66Yah and known to contribute to the synaptic meta-pathway group. After
415 performing a betweenness based centrality analysis on the joined Ts65Dn-Ts66Yah RegPPINet
416 we identified three main sub-networks (Fig. 7 A): the “HMC-immune response” gathered
417 members of the major histocompatibility complex (MHC) and of the IFN response, and is
418 almost Ts65Dn specific, whereas the two others, “RHO” and “Morphogenesis”, were more
419 affected in the Ts66Yah model. Furthermore, our network analyses here in Ts66Yah and
420 Ts65Dn support the role of the DS subnetworks linked to RHOA, SNARE proteins (Vamps and
421 Sec proteins interactors), DYRK1A and NPY (Fig. S11), which are deeply intertwined, as
422 previously identified in 7 other DS mouse models (DUCHON *et al.* 2021).
423 Then we focused on the EC and HIP Ts66Yah RegPPINet. Strikingly, the pathway dysregulation
424 in the EC unraveled a mild effect of the trisomic model over this tissue structure with 40
425 pathways affected, mainly morphogenesis, metabolism, cell structure and synaptic meta-
426 pathways (Fig 6; Fig. S12). The Ts66Yah EC RegPPINet built using all the meta-pathway
427 alterations revealed several well-connected subnetworks (Fig. S12B) linked mainly to
428 “morphogenesis”, “metabolism” and “host response & defense” (Fig. S12C). Conversely, a
429 more severe dysregulation with 323 altered pathways was revealed in the HIP (Table 4 and
430 S11, Fig S13A). Although less functional alteration was found in Ts66Yah than in Ts65Dn, the

431 stronger changes were found at the level of “Host response & defense” and “Metabolism”
432 meta-pathways with important relations with genes also belonging to morphogenesis and
433 synaptic related pathways (Fig. S13D). The network analysis identified several central genes
434 distributed over all the subnetworks (Fig. S13B, C) highlighting the strong connectivity and
435 importance of each subnetwork in the Ts66Yah HIP. Additionally, in the most closely
436 connected subnetwork including the top central genes, we identified *App* and G protein-
437 coupled receptor 3 for lysophosphatidic acid (LPA) *LPAR3* and *LPAR2*, which were closely
438 connected (Fig. S13C). Furthermore, most of the genes contributed to the alteration in
439 different meta-pathways or functionalities due to gene multifunctionality, again pointing out
440 the relevance of improving our understanding of comorbidity phenotypes in DS (Fig. S13D).
441

442 **DISCUSSION**

443 Here we report the general characterization of the new Ts66Yah line and compared several
444 outcomes with the well-known Ts65Dn DS mouse model. Ts66Yah is certainly more genetically
445 valid for DS studies than Ts65Dn as it does not contain trisomy of the *Scaf8-Pde10a*
446 centromeric Mmu17 region unrelated to Hsa21. The general transmission of the recombined
447 Ts66Yah chromosome was similar to the Ts65Dn, showing that the centromeric part of
448 Mmu17 does not play a major role in the sterility of trisomic males. The male germline
449 transmission property in the Ts66Yah may have arisen from the construction of the models
450 and should be monitored to see if it is maintained over generations. Interestingly, sperm
451 quality was also similar, thus probably the fertility issue is more connected to sperm fertility
452 as such rather than the parameters of concentration, mobility and velocity checked here.
453 More importantly, both DS models were found to replicate very classical DS cognitive features.
454 Similarities were found in behavior phenotypes in the two models for the nesting, object

455 recognition and spontaneous alternation tests. In particular, defects in object recognition
456 have been observed in many different labs for the Ts65Dn line and have been replicated in
457 two independent laboratories for Ts66Yah. Thus, we must consider this phenotype as a very
458 robust one, due to the trisomy of the region between *Mrpl39* and *Zbtb21* in mouse
459 chromosome 16. It would be very interesting to see if other phenotypes found in the Ts65Dn
460 are also reproduced in Ts66Yah. For example, the impairment in spatial learning was found in
461 the two models during the Morris water maze test but no spatial memory phenotype was
462 observed in Ts66Yah compared to Ts65Dn. In addition, we found that the Ts66Yah line did not
463 reproduce the anxiety and hyperactivity phenotypes observed in the open field with the
464 Ts65Dn line. Similarly, circadian activity was normal in Ts66Yah whereas we found increased
465 activity for Ts65Dn, as observed previously in light-dark condition (RUBY *et al.* 2010). Although
466 hyperactivity may be influenced by gene-environment interaction (ITOHARA *et al.* 2015),
467 increased locomotor activity is common to many mouse mutant models, i.e. 678 significant
468 genes out of 8641 mutants tested in the International Mouse Phenotyping consortium.
469 Hyperactivity could be a direct consequence of abnormal involuntary movement or motor
470 coordination, or indirect consequences, such as associated with stress, being in a novel
471 environment or being influenced when raised by or in contact with mutant individuals. This
472 increased activity has a major impact on behavioral testing in Ts65Dn, as shown recently by
473 the contribution of distance travelled and thigmotaxis to novel object discrimination (SIERRA *et*
474 *al.* 2021). This phenomenon should depend on genes located in Mmu17 either directly or
475 indirectly, because Ts66Yah was not affected. According to the Mouse Genome Informatics
476 database, mutants from five genes of the region, *Arid1b, Cep43, Nox3, Pde10a,* and *Serac1*,
477 are linked to activity, motor and stereotypic behavior and are strong candidates for which
478 overdosage may enhance the activity of the Ts65Dn mouse model. Similarities were also

479 observed in brain and craniofacial morphologies, with convergence found in both DS models.
480 Nonetheless, the severity of the trisomy in these two features were slightly different: The
481 Ts65Dn brain was larger than the Ts66Yah one in many different regions while the shape of
482 the cranium was affected differently, with more severe brachycephaly and increased mid-face
483 shortening in Ts66Yah, compared to Ts65Dn, a phenotype closer to human DS features.
484 Another intriguing result came from the expression analysis in the two brain regions, the HIP
485 and EC, which are both involved in learning and memory. First, there was little overlap in the
486 DEGs in the two models, and while some pathways were found dysregulated similarly in the
487 hippocampus of both models, no real pathway convergence was observed in the EC, with a
488 more severe impact for Ts65Dn compared to Ts66Yah, presumably due to the trisomy of the
489 centromeric region of Mmu17.
490 Altogether the results from learning and behavior, craniofacial and brain morphologies, and
491 gene expression in two brain regions, highlighted the interference of the *Scaf8-Pde10a*
492 trisomy in the Ts65Dn phenotypes. Considering the breeding of the two models on F1B6C3B,
493 it would be highly recommended to genotype for the zygosity of the *Scaf8-Pde10a* region that
494 can be found as heterozygous for B6 and C3B alleles, or homozygotes for both alleles. In
495 addition it would be important to control for any recombination event in the small region to
496 reduce the risk of generating a subline with specific genotype in this region. Interestingly some
497 gene like EZR, encoded in the Mmu17 interval, is known to interact with the RHOA pathway,
498 and is able to downregulate RHOA activity. Reversely, RHO can activate EZR activity and lead
499 to new specific phenotypes during neuritogenesis (YONEMURA *et al.* 2002; MATSUMOTO *et al.*
500 2014; HATANO *et al.* 2018). *EZR* was found to be a major hub in the top 5 influential genes,
501 considering both the betweenness index and the base mean expression levels. We may
502 therefore hypothesize that the EZR overexpression found in the Ts65Dn brain acts on the

503 downregulation of the RHOA pathway found altered in DS models (DUCHON *et al.* 2021). For
504 the low hyperactive phenotypes found in Ts66Yah compared to Ts65Dn, *Serac1 Pde10a* and
505 *Ccr6* are interesting candidates whose loss-of-function impaired locomotor activity while the
506 defect in *Kcne1* induced hyperactivity. This means that the variation in the dose of those genes
507 may explain the hyperactivity found to be more severe in Ts65Dn than in Ts66Yah.
508 In the network analysis of both the Ts65Dn and Ts66Yah hippocampi, we confirmed the
509 dysregulation in the immune response, RHOA and morphogenesis pathways, as detected
510 previously in several DS adult mouse models (DUCHON *et al.* 2021). From this common network,
511 five proteins, encoded by the Mmu16 region homologous to Hsa21, appeared to have stronger
512 effects, based on the betweenness centrality index (APP, SOD1, KCNJ6, SYNJ1, ITSN1) while
513 others had less impact (ATP5o, BACE2, BRWD1, DYRK1A, DSCAM, HLCS, IL10RB, INFAR2,
514 INFGR2, KCNE1, KCNE2, KCNJ15, MRPL39, MX2, OLIG2), supporting the multigenic dimension
515 in DS models. Interestingly, genes from other regions homologous to Hsa21 were also
516 detected in the hippocampal network, like COL6A1, COL6A2 and DNMT3L.
517 As the altered immune response in DS models has been reported previously (LING *et al.* 2014;
518 GUEDJ *et al.* 2016; DUCHON *et al.* 2021), we analyzed the gene cross-talk within all the
519 dysregulated pathways inside the "synaptic" and "host & immune response" meta-pathways.
520 We found that both meta-pathways were closely connected by protein-protein interaction
521 between several members and more interestingly, some of the genes had dual synaptic and
522 host response functionality such as *App, Cldn19, F2rl1* (involved in the behavioral neurological
523 phenotype)*, Ihh, Trpv1, Nppa, Wnt3a, Isl1,* and a few genes coding for cell adhesion molecules,
524 such as *H2-Q6* or *H2-Aa*.
525 Compared with the parental Ts65Dn, the Ts66Yah line revealed the importance of the *Scaf8-*
526 *Pde10a* trisomy. Interestingly this region varies quite often in the mouse genetic inbred

527 backgrounds used to generate and maintain the Ts65Dn minichromosome. Unfortunately, the
528 follow-up of the alleles in this region has never been done although there was a proposal to
529 use a SNP in *Snx9* to detect the DBA/2J allele in the Ts65Dn minichromosome (LORENZI *et al.*
530 2010). This increased variation may contribute to the fluctuation of the phenotypes observed
531 from stocks to stocks in the Ts65Dn (SHAW *et al.* 2020). More importantly, our study
532 demonstrates that, in mouse models, DS related phenotypes could be altered by change in
533 genetic dosage of another genomic region, the *Scaf8-Pde10a* genetic interval. Conversely, this
534 region may change penetrance or expressivity of features in individual with DS. Indeed, the
535 *SCAF8-PDE10A* on human chromosome 6 is also subjected to copy number variation according
536 to the DECIPHER database (FIRTH *et al.* 2009). In human, the region is rearranged in the 3' part
537 (Fig S1B) and contains several morbid genes. Notably, ARID1B encodes a subunit of the
538 chromatin remodeling complex SWI/SNF-A, and is linked with heterozygous dominant
539 mutation to the Coffin-Siris syndrome (www.orpha.net; ORPHA:1465) and with deletion to the
540 6q25 haploinsufficiency syndrome (ORPHA: 251056). *SERAC1* deficiency leads to MEGDEL
541 syndrome with autosomal recessive mutations affecting neonates with hypoglycaemia,
542 feeding problem, hypotonia, sepsis-like clinical picture without infection (ORPHA: 352328).
543 Recessive mutations of *GTF2H5*, coding for a subunit of transcription/repair factor TFIIH, lead
544 to trichothiodystrophy (ORPHA:33364). Similarly, *RSPH3* is involved of primary ciliary
545 dyskinesia (ORPHA:244), and *PDE10A* involved in two infantile movement disorders
546 (ORPHA:494541 and 494526). Thus, the additional trisomy of *Scaf8-Pde10a* has a strong effect
547 on the expression of several DS related features in models. This phenomenon of additive
548 effect due to genetic interaction has been observed in other copy number variation diseases
549 (PIZZO *et al.* 2019). Overall it highlights the need of complete evaluation of the genetic
550 background in individual with DS, to define potential interaction with other candidate disease-

551 associated variants and to get a better understanding of the DS complexity. Our report
552 introduced a new model with a freely segregating chromosome with a stronger genetic validity
553 for DS, phenotypic variation in 3 main areas affected in individual with DS. Therefore, we hope
554 that the DS research community will consider working with the newTs66Yah mouse model for
555 DS, although this model remains partial DS model since the triplicated *Mrpl39* to *Zbtb21* region
556 encompass 102/187 of the Hsa21 orthologous protein coding genes. The Ts66Yah model
557 should be reduce interference with the Mmu17 region unrelated to Hsa21 in Ts65Dn, and
558 obtain more refine analysis of DS during lifetime, closer to the DS genetic condition.
559

560 **MATERIALS AND METHODS**

561 All the experiments were performed in accordance with the Directive of the European
562 Parliament: 2010/63/EU, revising/replacing Directive 86/609/EEC and with French Law
563 (Decreet no. 2013-118 01 and its supporting annexes which came into force on 1 February
564 2013) relating to the protection of animals used in scientific experimentation. YH was the
565 principal investigator of this study (accreditation 67-369) in our animal facility (Agreement
566 C67-218-40). Experimental procedures for the use of animals for research were approved by
567 the Ministry of National Education, Higher Education and Research and with the agreement
568 of the local ethical committee Com'Eth (no. 17) under the accreditation number
569 APAFIS#13127-2018012210465339 v5 and APAFIS#21969-2019091215444738 v3.
570

571 **Mouse lines**

572 The trisomic Ts65Dn (Ts(17^{16})65Dn) mice, initially obtained from the Jax, was kept in an F1
573 B6C3B genetic background (with the C3B line as a C_3H/HeH congenic line for the BALB/c allele
574 at the *Pde6b* locus (HOELTER *et al.* 2008). Ts65Dn mice were genotyped according to published

575 protocols (DUCHON *et al.* 2011a). Two primers were selected on both sides of the breakpoint
576 to amplify a fragment of 396 bp (with forward primer Fw_wtTs65Dn:
577 GACTTAGTAAGAGCAAGTGGC and reverse primer Rev_Ts65Dn:
578 AGGTAGAAAGATGTGAGGACAC), and a third primer was designed on the reverse strand of
579 chromosome 17 to amplify a fragment of 290 bp (GGGCAACACTGGATCAATC).
580 The generation of the new mouse line was done at the Mouse Clinical Institute. Briefly, Ts65Dn
581 male mice were selected and used for in vitro fertilization to produce fertilized eggs that were
582 injected with two pairs of gRNAs (Fig. 1A) with one pair located on the centromeric region of
583 Mmu17 and the other in the proximity of the breakpoint in the Ts65Dn minichromosome and
584 on the Mmu16 region (for details see supplementary information). The recombined
585 chromosome was selected to propagate upon breeding. As such the full name of the mouse
586 line should be Ts66YahIcs, shortened here to Ts66Yah.
587 Ts66Yah mice were genotyped with a specific primer encompassing the new break point
588 between Mmu17 and Mmu16, with a forward primer Ts66Yah_wt-tg_up
589 (GGAAATATCGCACTTCACCAA) and a reverse primer Ts66Yah_tg_dw
590 (CATGGGTCTGTGTGGTTTTCT) to amplify a fragment of 322 bp. A third reverse primer was
591 designed on the reverse strand of chromosome 16 to amplify a wt fragment of 234 bp
592 (TCTAGGATCAGTGGGACTTTTGT).
593 Metaphase spread. Fibroblasts obtained from Ts66Yah were treated with 0.02 µg/ml
594 colcemide for 2 h. Cells were then trypsinized, and the cell pellet was incubated in 0.56 % KCl
595 for 20 min in 5 % CO2 at 37 °C (hypotonic shock). Cells were then fixed in methanol-acetic acid
596 3V/1V for 20 min at room temperature, then washed three times with methanol-acetic acid
597 and concentrated in a small volume. Drops of cell suspension were then plated on glass slides

598 at 50 °C. The cells were then allowed to dry and stained with Giemsa 4 % as described
599 previously (CODNER *et al.* 2016).
600 CGH. To confirm the increased copy number, we performed a comparative genomic
601 hybridization (CGH) of the Ts65Dn and Ts66Yah models with their wild-type controls.
602 Comparative analysis was done using DNA extracts from one wild-type and one trisomic
603 animal that were fluorescently labeled. After labeling, DNA was hybridized to CGH array.
604 Finally, the slides were scanned and the array images analyzed (for details, see supplementary
605 information CGH array).
606
607 **Sperm Analysis**
608 Sperm analysis was done with IVOS (Hamilton Thorne) apparatus. After euthanasia, the vasa
609 deferentia and cauda epididymis were dissected and sperm was sampled. The quality and
610 quantity of semen was estimated according to four main parameters: concentration
611 (millions/ml), motility (%), rapid cells (%) and progressivity (%). For this analysis, sperm was
612 diluted 20 times in prewarm (37°C) COOK solution (COOK ®, ref K-RVFE-50 COOK France). The
613 suspension was gently agitated and placed for 3 to 4 minutes in a CO2 incubator before
614 analysis with the IVOS system.
615
616 **Behavior pipeline**
617 We generated several experimental animal cohorts by selecting mice from litters containing a
618 minimum of two male pups. One cohort was used for nesting activity, working memory in the
619 Y maze, exploration of a novel environment in the open-field, spatial memory in the Morris
620 water maze, and circadian activity. Three independent cohorts of animals were used for
621 sperm, cranio-facial analysis and object recognition memory. Moreover, we also confirmed

622 some phenotypes in another laboratory with a complete independent group of mice (17 males
623 and 15 females 2n compared to 11 males and 14 females Ts66Yah). Independently of this line,
624 a cohort of Ts65Dn mice was also built and assessed in the same behavioral pipeline, in order
625 to permit direct comparison of both lines.
626 After weaning, animals were sorted by litters into 39 x 20 x 16 cm cages (Green Line,
627 Techniplast, Italy) where they had free access to purified water and food (D04 chow diet, Safe,
628 Augy, France). The temperature was maintained at 23±1 °C and the light cycle was controlled
629 as 12 h light and 12 h dark (lights on at 7 am). On testing days, animals were transferred to
630 the antechambers of the experimental room 30 min before the start of the experiment. All
631 the experiments were performed between 8:00 AM and 4:00 PM. A resting period of 2 days
632 to 1 week was used between two consecutive tests.
633 A series of behavioural experiments were conducted on male mice with ages ranging from 1.8
634 months on starting to 4.5 months for the last test. The tests were administered in the following
635 order: Circadian activity, nesting, Y-maze, square open field, open field, novel object
636 recognition, Morris water maze (standard hidden and reversal) and fear conditioning
637 (contextual and cue). Behavioral experimenters were blinded to the genetic status of the
638 animals. All the tests were performed with the experimenter out of the animal's sight. Further
639 experiments for the evaluation of the spontaneous alternation and NOR made in a different
640 laboratory (Fig. S5), where the two sexes were evaluated.
641
642 **Circadian activity**
643 Circadian activity (CA) was measured to assess spontaneous activity behavior over the
644 complete light/dark cycle. The actimeter (Imétronic, Pessac, France) is composed of 8
645 individual boxes (11 x 21 x 18 cm3), each of them equipped with an array of four parallel

646 horizontal infrared beams and linked to a computer allowing recordings of photocell beam
647 breaks, providing automated measures of position and locomotor activity. Mice were put into
648 cages at 11 am on the first day and removed the next day at 7 pm. The light cycle was
649 controlled as 12 h light and 12 h dark (lights on at 7 am). The 32 hours of testing were divided
650 into three different phases: the habituation phase (from 11 am to 7 pm on the first day); the
651 night/dark phase (from 7 pm on the first day to 7 am on the second day); and the day/light
652 phase (from 7 am to 7 pm on the second day).
653
654 **Nesting**
655 This test was performed by placing the mice individually in clean new housing cages two hours
656 before the dark phase and the results were assessed the next morning. Normal bedding
657 covered the floor to a depth of 0.5 cm. Each cage was supplied with a 'Nestlet', a 5 cm square
658 of pressed cotton batting. The nests were assessed on a 5-point scale. 1- The Nestlet was
659 largely untouched (>90% intact). 2- The Nestlet was partially torn up (50-90% remaining
660 intact). 3- The Nestlet was mostly shredded but often there was no identifiable nest site: <
661 50% of the Nestlet remained intact but < 90% was within a quarter of the cage floor area, i.e.
662 the cotton was not gathered into a nest but spread around the cage. 4- An identifiable but flat
663 nest: > 90% of the Nestlet was torn up, the material was gathered into a nest within a quarter
664 of the cage floor area, but the nest was flat with walls higher than mouse body height (curled
665 up on its side) on less than 50% of its circumference. 5- A (near) perfect nest: > 90% of the
666 Nestlet was torn up, the nest was a crater, with walls higher than mouse body height for more
667 than 50% of its circumference (DEACON 2006).
668
669 **Y-maze**

670 Short-term memory was assessed by recording spontaneous alternation in the Y-maze test
671 (HUGHES 2004). The Y-maze test is based on the innate preference of animals to explore an arm
672 that has not been explored previously, a behavior that, if occurring with a frequency greater
673 than 50%, is called spontaneous alternation behavior (SAB). The maze was made of three
674 enclosed plastic arms, each 40x9x16cm, set at an angle of 120° to each other in the shape of
675 a Y. The wall of each arm had a different pattern to encourage SAB. Animals were placed at
676 the end of one arm (this initial arm was alternated within the group of mice to prevent arm
677 placement bias), facing away from the center, and allowed to freely explore the apparatus for
678 8 min under moderate lighting conditions (70 lux in the center-most region). The time
679 sequences of entries in the 3 arms were recorded, (considering the mouse enters an arm when
680 all four paws were inside the arm). Alternation was determined from successive entries into
681 the three arms on overlapping triplet sets in which three different arms are entered. The
682 number of alternations was then divided by the number of alternation opportunities, namely,
683 total arm entries minus one. In addition, total entries were scored as an index of locomotor
684 activity.
685
686 **Adaptation to a novel environment under stressful conditions**
687 A square open-field (OF) was used to evaluate mice adaptation to a novel environment under
688 stressful conditions. Mice were tested in an automated square OF (44.3 x 44.3 x 16.8 cm) made
689 of PVC with transparent walls, a black floor, and covered with translucent PVC (Panlab,
690 Barcelona, Spain). The open field arena was divided into central and peripheral regions and
691 was homogeneously illuminated at 150 Lux. Each mouse was placed on the periphery of the
692 open field and allowed to explore the apparatus freely for 30 min. The distance travelled, the
693 number of rearing episodes, and the stereotypes in the central and peripheral zones were

694 recorded over the 30 min test session. Stereotypes is the number of samples where the
695 position of the subject is different from its position during the previous sample and equal to
696 its position during the 2nd sample back in time. The distance is the total distance (cm) travelled
697 in the corresponding zone.
698
699 **Novel Object Recognition (NOR)**
700 The novel object recognition task is based on the innate tendency of rodents to explore novel
701 objects over familiar ones (BEVINS and BESHEER 2006). This test was done 24 hours after the last
702 OF session performed in the same arena. On Day 1, mice were free to explore 2 identical
703 objects for 10 min. After this acquisition phase, mice returned to their home cage for a 24-
704 hour retention interval. Their memory was evaluated on day 2, using one familiar object (of
705 those already experienced during the acquisition phase) and one novel object which were
706 placed in the arena with the mice free to explore the two objects for a 10 min period. Between
707 trials and subjects, the different objects were cleaned with 70° ethanol to reduce olfactory
708 cues. To avoid a preference for one of the two objects, the new one was different and
709 counterbalanced between the different animal groups and genotypes. Similarly, to avoid a
710 location preference, the emplacement of the novel object compared to the familiar one (left
711 or right) was counterbalanced too. Object exploration was manually scored and defined as the
712 orientation of the nose to the object, allowing a distance < 1 cm. For the retention phase, the
713 percentage of time exploring familiar vs novel objects was calculated to assess memory
714 performance.
715
716 **Morris Water Maze (MWM)**

717 Spatial learning can be analyzed using the MWM task. This test was designed for the animals
718 to learn to navigate a swimming tank (150 cm of diameter) filled with opaque water, following
719 the most direct path to a hidden submerged platform when starting from different, random
720 locations around the perimeter of the tank. The use of distal cues provides the most effective
721 strategy to accomplish this task and avoid the aversive effect of cold water (22°C). This ability
722 is controlled by hippocampal-dependent spatial cognition. The partially trisomic mice were
723 trained in the standard version of the water maze as previously described (VORHEES and
724 WILLIAMS 2006; ARBOGAST *et al.* 2015). This standard version contains 2 different phases, a
725 learning phase (using 7 acquisition sessions) and a probe test (to assess memory
726 performance). At the end of this standard version, memory flexibility was tested with a
727 reversal phase, in which the PF was positioned in the opposite quadrant (using 4 acquisition
728 sessions) and a probe test. Reversal learning in the MWM reveals whether or not animals can
729 extinguish their initial learning and acquire a direct path to the new goal position. Finally, a
730 cue session was done to validate the test. All the trials were recorded with a video tracking
731 system (Ethovision, Wageningen, Netherlands). The swim paths for each mouse in each trial
732 of the MWM test were categorized manually into one of the following search strategies (see
733 supplementary information MWM).
734
735 **Fear conditioning (Contextual and Cued)**
736 To further challenge hippocampus mediated cognitive behaviors we used the fear
737 conditioning test. Fear conditioning (FC) is an associative learning paradigm for measuring
738 aversive learning and memory where a neutral conditioned stimulus (CS) such as light and
739 tone are paired with an aversive unconditioned stimulus (US) such as mild shock to the paw.
740 Animals associate the spatial context cues with the CS concomitantly. After conditioning, the

741 CS or the spatial context elicits a central state of fear in the absence of the US, translated into
742 a reduced locomotor activity or total lack of movement (freezing) response (see
743 supplementary information FC). Thus, immobility time is used as a measure of
744 learning/memory performances (CRAWLEY 1999; GOELDNER *et al.* 2009).
745
746 **Statistical analysis**
747 For each data set, we performed the Shapiro–Wilk test and Quantile-Quantile plots to, analyze
748 if the data were normally distributed and the Brown-Forsythe test to ascertain the
749 homogeneity of variances. Statistical significance of differences between groups was inferred
750 by a T test between genotype or ANOVA for repeated measures (MWM, FC). The post hoc
751 tests (Tukey Test) were conducted only if F in RMANOVA achieved a 0.05 level. In the case of
752 datasets where the assumptions of normality or homogeneity of variances were not fulfilled,
753 we performed the Kruskal-Wallis non-parametric test. For the NOR, Y-maze and probe test in
754 MWM, we also performed a one sample t-test on the RI or on the percentage of spontaneous
755 alternation versus 0, 50% or 25% respectively (hazard). In addition, for the Y-maze and the
756 NOR, we performed a one sample t test versus 50% (the randomness probability) for the % of
757 alternation and the sniffing time for the NO, for the two genotypes.
758
759 **Identify further the explanatory phenotyping variables in the trisomic lines**
760 We developed "Gdaphen" for "Genotype discrimination using phenotypic features" as an R
761 pipeline that allows the identification of the most important predictive qualitative and
762 quantitative variables for genotype discrimination in phenotypic based datasets without any
763 prior hypothesis (available on github https://github.com/YaH44/GDAPHEN). Gdaphen was
764 based on two classification methods, the first one used the Generalized Linear Model (GLM)

765 while the second used Random Forest Classification (RFC), to identify the explanatory
766 phenotypic variables that allow discriminating between the 2 models without forcing the
767 variables to follow a linear relationship in the comparison between trisomic and wild-type
768 individuals, as in the first GLM-based one. Moreover, we also searched for another set of
769 relevant variables to discriminate each model (Ts65Dn versus Ts66Yah) to obtain deeper
770 understanding of the differences in these mice models. The Gdaphen pipeline was built using
771 several available R packages (Supplementary information) to identify the discriminating
772 phenotypic variables according to the genotypes analyzed. Gdaphen takes as input data a
773 table containing information per animal in the rows and all the variables recorded in each
774 column. Several variables were recorded and grouped using the same group label to identify
775 the importance for the discrimination of: i) each variable alone, ii) the overall contribution of
776 the group. Pre-processing steps were carried out to get the data into shape for the analysis
777 (see suppl. Material methods), after which Gdaphen was able to first identify the highly
778 correlated variables (more than a r=0.75) and remove them for downstream analysis. For
779 example, in the sperm tests several variables measured for the test were highly correlated
780 with each other. The sperm percentage of rapid cells and the percentage of cell motility
781 showed a coefficient of correlation r=0.987. Similarly, the percentage of rapid spermatozoa
782 (“Sperm:Rapid_cells “) was 0.97 correlated with the “percentage of progressive cells
783 (“Sperm:Progressive"). Thus, we decided to keep only the two variables: the sperm
784 concentration (“Sperm:C°”, millions/ml)” and the percentage of progressive
785 cells(“Sperm:Progressive").
786 We decided to use two different classifiers to answer two different questions: I) a GLM or
787 GLM-Net model that will allow us to identify which phenotypic variables or “predicting
788 variables” are able to discriminate due to the fact that their linear combination influences the

789 value of the dependent variable response; II) a random forest, noted RF, unsupervised
790 algorithm that will be able to identify relevant phenotypic variables for the discrimination
791 even though they may not originate from a linear distribution or exponential distribution
792 family or have a linear relationship. Both functions are taken from the caret R and nnet R
793 packages.
794 This method is able to deal with groups of both qualitative and quantitative variables recorded
795 from the same individuals. The MFA performs a normalization or "weighting" on each group
796 by dividing all the variables belonging to the group by the first eigenvalue from the principal
797 component analysis (PCA) of the group. Then a PCA on all the weighted variables is applied so
798 we can identify the correlation between the grouped or ungrouped qualitative or quantitative
799 variables, the principal component dimensions, and identify the individual coordinates of each
800 observation on the PCA dimensions. The method is implemented using the MFAmix function
801 from the PCAmixdata R package. Moreover, we chose a vectorization visualization approach
802 like that implemented in PCAmixdata where we included the cosine similarity distance to
803 further highlight the parameters that follow the same trajectory as Genotype. Consequently,
804 these parameters contribute to the separation of the individual data on the same dimensions
805 defined by their cosine similarity distance. We analyzed three different numbers of phenotypic
806 predictor variables: i) all phenotypic variables; ii) the phenotypic variables left after removing
807 the highly correlated ones (correlation higher than 75%); and iii) the phenotypic variables
808 contributing more than a 30% in the discrimination after running the MFA analysis using all
809 the variables and observing the correlation between the quantitative ungrouped phenotypic
810 variables with the main three dimensions of the PCA. Our reasoning is to try to decrease the
811 noise added by variables that do not strongly contribute to the discrimination, decrease the
812 complexity of the model and the calculations, and increase the power on the discrimination

813 since a lower number of variables are considered. Then we calculated the variance of the data
814 that we were able to explain using the first 10 dimensions and the accuracy of the models to
815 answer how well they can correctly predict each individual observation in the class of the
816 dependent variable. We ran the Gdaphen pipeline to perform the genotype discrimination
817 analyses on: 1) Ts65Dn mutants and controls; 2) Ts66Yah mutants and their respective
818 controls; 3) Ts65Dn and Ts66Yah mutants and their respective control phenotypic data. In all
819 these analyses, the model built using the phenotypic predictor variables known to contribute
820 more than 30% to the discrimination was always able to explain a higher percentage of the
821 variance in the data.
822
823 **Magnetic Resonance Imaging**
824 A dedicated cohort of animals at age 102 +/- 7 days was anesthetized and perfused with 30
825 ml of room temperature 1X Phosphate Buffer Saline (PBS) supplemented with 10% (% w/v)
826 heparine and 2mM of ProHance Gadoteridol (Bracco Imaging, Courcouronnes, France)
827 followed by 30ml of 4% PFA supplemented with 2mM of ProHance Gadoteridol. Then the brain
828 structure was dissected and kept in PFA 4% 2mM ProHance overnight at 4°C. The next day,
829 each specimen was transferred into 1X PBS 2mM ProHance until imaging. Just prior to
830 imaging, the brains were removed from the fixative and placed in plastic tubes (internal
831 diameter 1 cm, volume 13 mL) filled with a proton-free susceptibility-matching fluid
832 (Fluorinert® FC-770, Sigma-Aldrich, St. Louis, MO). Images of excised brains were acquired on
833 a 7T BioSpec animal MRI system (Bruker Biospin MRI GmbH, Ettlingen, Germany).
834 Morphological MRI images were compared across groups with a region-based analysis. The
835 resulting region-based volume estimations were averaged out for each animal before the
836 statistical analysis (see supplementary information MRI).

837

838 **Morphometrics**

839 Mice used for the craniofacial study were sacrificed at 18 weeks of age and carcasses were
840 skinned, eviscerated and store in Ethanol 96%. Cranium morphology was assessed using the
841 Quantum µCT scanner (Perkin Elmer, Whaltham, USA). All scans were performed with an isotropic
842 voxel size of 20 µm, 160 µA tube current and 90 kV tube voltage. We applied a common approach
843 to shape analysis named geometric morphometrics GM using the Geomorph software
844 package in the R statistical computing environment (ADAMS AND OTÁROLA-CASTILLO 2013). This
845 approach used the coordinates of 39 relevant cranial landmarks that were recorded using
846 Landmark software (Institute for Data Analysis and Visualization (IDAV) group at the University
847 of California, Davis, Table S3). This step permitted recording the relative positions of
848 morphological points, boundary curves and surfaces as the basis of shape quantification. A
849 generalized Procrustes analysis was then used to superimpose the specimens on a common
850 coordinate system by holding their position, size and orientation constant. From the
851 Procrustes-aligned coordinates, a set of shape variables was obtained which can be used in
852 multivariate statistical analyses. Graphical methods were used to visualize patterns of shape
853 variation. For example, the shape differences between groups could be visualized graphically
854 by obtaining the average landmark coordinates for each group and the overall mean, and
855 plotting the differences as thin-plate spline transformation grids. Taking a different approach,
856 the principal component analysis (CPA) is a mathematical procedure that transforms a number
857 of correlated variables into a number of uncorrelated variables. This permitted visualizing
858 patterns of shape variation in shape space.

859

860 **QRT-PCR**

861 cDNA synthesis was performed using the SuperScript® VILO™ cDNA Synthesis Kit (Invitrogen,
862 Carlsbad, CA). PCRs were performed with TaqMan® Universal Master Mix II and pre-optimized
863 TaqMan® Gene Expression assays (Applied Biosystems, Waltham, Massachusetts, USA),
864 consisting of a pair of unlabeled PCR primers and a TaqMan® probe with an Applied
865 Biosystems™ FAM™ dye label on the 5' end and minor groove binder (MGB) and
866 nonfluorescent quencher (NFQ) on the 3' end (listed in Supplementary Table 4). mRNA
867 expression profiles were analyzed by real-time quantitative PCR using TaqMan TM universal
868 master mix II with UNG in a realplex II master cycler, Eppendorf (Hamburg, Germany). The
869 complete reactions were subjected to the following program of thermal cycling: 1 cycle of 2
870 minutes at 50°C; 1 cycle of 10 minutes at 95°C; 40 cycles of 15 seconds at 95°C and 1 minute
871 at 60°C. The efficiencies of the TaqMan assays were checked using cDNA dilution series from
872 extracts of hippocampal sample. Normalization was performed by amplifying 4 housekeeping
873 genes (*Gnas, Pgk1, Actb* and *Atp5b*) in parallel and using the GeNorm procedure to correct the
874 variations of the amount of source RNA in the starting material (39). All the samples were
875 tested in triplicate.
876
877 **Gene expression analyses**
878 The hippocampus and entorhinal cortex from 6 Ts65Dn and 6 control littermates and 6
879 Ts66Yah and 5 control littermates were isolated and flash frozen in liquid nitrogen. Total RNA
880 was prepared using an RNA extraction kit (Qiagen, Venlo, Netherlands) according to the
881 manufacturer's instructions. Sample quality was checked using an Agilent 2100 Bioanalyzer
882 (Agilent Technologies, Santa Clara, California, USA). All the procedures and the analysis are
883 detailed in the supplementary information.

884 The preparation of the libraries was done by the GenomEast platform, a member of the
885 'France Génomique' consortium (ANR-10-INBS-0009), using the TruSeq Stranded Total RNA
886 Sample Preparation Guide - PN 15031048. Total RNA-Seq libraries were generated from a
887 minimum of 150-300 ng of total RNA using TruSeq Stranded Total RNA LT Sample Prep Kit with
888 Ribo-Zero Gold (Illumina, San Diego, CA), according to the manufacturer's instructions.
889 The molecules extracted from the biological material were polyA RNA. Whole genome
890 expression sequencing was performed by the platform using Illumina Hiseq 4000 and
891 generating single end RNA-Seq reads of 50 bps length. The raw sequenced reads were aligned
892 by Hisat2 against the GRCm38.v99 mouse assembly. 55385 ENSEMBL Gene Ids were
893 quantified aligning with the GRCm38.v99 assembly. HTSeq-count was used to generate the
894 raw counts. The downstream analyses were carried on with in-house bash scripts and R
895 version 3.6 scripts using FCROS (Dembele et al., 2014) and DESeq2 (Love et al., 2014) packages
896 to identify the DEGs. Raw reads and normalized counts have been deposited in GEO (Accession
897 No. GSExxxxx).
898 We performed the functional differential analysis (LUO *et al.* 2009) and grouped all the
899 pathways into 25 functional categories (noted meta-pathways). Then, to assess gene
900 connectivity we built a minimum fully connected protein-protein interaction (PPI) network
901 (noted MinPPINet) of genes known to be involved in the synaptic function as they were
902 associated with synaptic pathways via the GO (ASHBURNER *et al.* 2000) and KEGG databases
903 (ESLING *et al.* 2015). Regulatory information was also added to build the final RegPPINet. We
904 used the betweenness centrality analysis to identify hubs, keys for maintaining the network
905 communication flow.

906 **Identification of central genes in the occurrence of behavioral phenotypes**

907 To further study the genotype-phenotype relationship in those models we combined the
908 behavioral results and the RNA-Seq data to identify central genes altered in the models and
909 linked to the phenotypes observed using the genotype-phenotype databases GO, KEGG and
910 DisGeNET.
911 First, we downloaded the list of experimentally validated genes known to be involved in
912 hyperactivity or locomotion behavior from the human disease database DIsGeNET (dataset:
913 Hyperactive behavior, C0424295 with 1263 genes) and annotated the genes with a high
914 confidence ortholog in mouse. We added all the mouse genes involved in GO genesets linked
915 to locomotion or motor behavior (18 GO terms: GO:0007626, GO:0008344, GO:0031987,
916 GO:0033058, GO:0035641, GO:0040011, GO:0040012, GO:0040013, GO:0040017,
917 GO:0043056, GO:0045475, GO:0090325, GO:0090326, GO:0090327, GO:1904059,
918 GO:1904060, GO:0036343, GO:0061744). Then, we queried our RNA-Seq data for these genes
919 to identify those found deregulated in the datasets.
920
921 **ACKNOWLEDGMENTS**
922 We would like to thank the members of the research group, of the IGBMC laboratory and of
923 the ICS for their help in brain morphometric analysis. We extend our thanks to the animal
924 caretakers of the ICS who are in charge of mice well-being. This work was supported by the
925 Jérôme Lejeune foundation. We acknowledge the Sisley-d'Ornano and Jérôme Lejeune
926 Foundations that awarded MF with a postdoctoral fellowship.
927 This work was supported by the National Centre for Scientific Research (CNRS), the French
928 National Institute of Health and Medical Research (INSERM), the University of Strasbourg
929 (Unistra), French government funds through the "Agence Nationale de la Recherche" in the
930 framework of the Investissements d'Avenir program [ANR-10-IDEX-0002-02, ANR-10-LABX-

0030-INRT, ANR-10-INBS-07 PHENOMIN to YH] and also provided by the Joint Programming Initiative Neurodegenerative Diseases (JPND) multinational research project HEROES (ANR-17-JPCD-0003). This project received funding from the European Union's Horizon 2020 research and innovation program under grant agreement GO-DS21 No 848077. The funders had no role in the study design, data collection and analysis, decision to publish, or preparation of the manuscript.

942 **REFERENCES**

943 Arbogast, T., M. Raveau, C. Chevalier, V. Nalesso, D. Dembele *et al.*, 2015 Deletion of the App-Runx1
944 region in mice models human partial monosomy 21. Disease Models & Mechanisms 8**:** 623-
945 634.
946 Ashburner, M., C. A. Ball, J. A. Blake, D. Botstein, H. Butler *et al.*, 2000 Gene ontology: tool for the
947 unification of biology. The Gene Ontology Consortium. Nat Genet 25**:** 25-29.
948 Aziz, N. M., F. Guedj, J. L. A. Pennings, J. L. Olmos-Serrano, A. Siegel *et al.*, 2018 Lifespan analysis of
949 brain development, gene expression and behavioral phenotypes in the Ts1Cje, Ts65Dn and
950 Dp(16)1/Yey mouse models of Down syndrome. Dis Model Mech 11.
951 Aït Yahya-Graison, E., J. Aubert, L. Dauphinot, I. Rivals, M. Prieur *et al.*, 2007 Classification of human
952 chromosome 21 gene-expression variations in Down syndrome: impact on disease
953 phenotypes. Am J Hum Genet 81**:** 475-491.
954 Bevins, R. A., and J. Besheer, 2006 Object recognition in rats and mice: a one-trial non-matching-to-
955 sample learning <p>task to study 'recognition memory. Nat Protoc 1**:** 1306-1311.
956 Codner, G. F., L. Lindner, A. Caulder, M. Wattenhofer-Donze, A. Radage *et al.*, 2016 Aneuploidy
957 screening of embryonic stem cell clones by metaphase karyotyping and droplet digital
958 polymerase chain reaction. BMC Cell Biol 17**:** 30.
959 Cohen, S. J., and R. W. Stackman, 2015 Assessing rodent hippocampal involvement in the novel object
960 recognition task. A review. Behav Brain Res 285**:** 105-117.
961 Concordet, J. P., and M. Haeussler, 2018 CRISPOR: intuitive guide selection for CRISPR/Cas9 genome
962 editing experiments and screens. Nucleic Acids Res 46**:** W242-W245.
963 Crawley, J. N., 1999 Behavioral phenotyping of transgenic and knockout mice: experimental design and
964 evaluation of general health, sensory functions, motor abilities, and specific behavioral tests.
965 Brain Research 835**:** 18-26.
966 Davisson, M. T., C. Schmidt and E. C. Akeson, 1990 Segmental trisomy of murine chromosome 16: a
967 new model system for studying Down syndrome. Prog Clin Biol Res 360**:** 263-280.
968 Davisson, M. T., C. Schmidt, R. H. Reeves, N. G. Irving, E. C. Akeson *et al.*, 1993 Segmental trisomy as a
969 mouse model for Down syndrome. Prog Clin Biol Res 384**:** 117-133.
970 Deacon, R. M. J., 2006 Digging and marble burying in mice: simple methods for in vivo identification of
971 biological impacts. Nature Protocols 1**:** 122-124.
972 Duchon, A., M. Del Mar Muñiz Moreno, S. M. Lorenzo, M. P. S. de Souza, C. Chevalier *et al.*, 2021 Multi-
973 influential genetic interactions alter behaviour and cognition through six main biological
974 cascades in Down syndrome mouse models. Hum Mol Genet.
975 Duchon, A., and Y. Herault, 2016 DYRK1A, a Dosage-Sensitive Gene Involved in Neurodevelopmental
976 Disorders, Is a Target for Drug Development in Down Syndrome. Front Behav Neurosci 10**:** 104.
977 Duchon, A., M. Raveau, C. Chevalier, V. Nalesso, A. J. Sharp *et al.*, 2011a Identification of the
978 translocation breakpoints in the Ts65Dn and Ts1Cje mouse lines: relevance for modeling Down
979 syndrome. Mamm Genome 22**:** 674-684.
980 Duchon, A., M. Raveau, C. Chevalier, V. Nalesso, A. J. Sharp *et al.*, 2011b Identification of the
981 translocation breakpoints in the Ts65Dn and Ts1Cje mouse lines: relevance for modeling down
982 syndrome. Mammalian Genome 22**:** 674-684.
983 Esling, P., F. Lejzerowicz and J. Pawlowski, 2015 Accurate multiplexing and filtering for high-throughput
984 amplicon-sequencing. Nucleic Acids Res 43**:** 2513-2524.
985 Faundez, V., I. De Toma, B. Bardoni, R. Bartesaghi, D. Nizetic *et al.*, 2018 Translating molecular advances
986 in Down syndrome and Fragile X syndrome into therapies. Eur Neuropsychopharmacol 28**:**
987 675-690.
988 Fernandez, F., W. Morishita, E. Zuniga, J. Nguyen, M. Blank *et al.*, 2007 Pharmacotherapy for cognitive
989 impairment in a mouse model of Down syndrome. Nat Neurosci 10**:** 411-413.

990 Firth, H. V., S. M. Richards, A. P. Bevan, S. Clayton, M. Corpas *et al.*, 2009 DECIPHER: Database of
991 Chromosomal Imbalance and Phenotype in Humans Using Ensembl Resources. Am J Hum
992 Genet 84**:** 524-533.
993 García-Cerro, S., N. Rueda, V. Vidal, S. Lantigua and C. Martínez-Cué, 2017 Normalizing the gene dosage
994 of Dyrk1A in a mouse model of Down syndrome rescues several Alzheimer's disease
995 phenotypes. Neurobiol Dis 106**:** 76-88.
996 Goeldner, C., D. Reiss, J. Wichmann, B. L. Kieffer and A.-M. Ouagazzal, 2009 Activation of nociceptin
997 opioid peptide (NOP) receptor impairs contextual fear learning in mice through glutamatergic
998 mechanisms. Neurobiology of Learning and Memory 91**:** 393-401.
999 Goodliffe, J. W., J. L. Olmos-Serrano, N. M. Aziz, J. L. Pennings, F. Guedj *et al.*, 2016 Absence of Prenatal
1000 Forebrain Defects in the Dp(16)1Yey/+ Mouse Model of Down Syndrome. J Neurosci 36**:** 2926-
1001 2944.
1002 Guedj, F., J. L. Pennings, L. J. Massingham, H. C. Wick, A. E. Siegel *et al.*, 2016 An Integrated
1003 Human/Murine Transcriptome and Pathway Approach To Identify Prenatal Treatments For
1004 Down Syndrome. Sci Rep 6**:** 32353.
1005 Hatano, R., A. Takeda, Y. Abe, K. Kawaguchi, I. Kazama *et al.*, 2018 Loss of ezrin expression reduced the
1006 susceptibility to the glomerular injury in mice. Sci Rep 8**:** 4512.
1007 Heller, H. C., A. Salehi, B. Chuluun, D. Das, B. Lin *et al.*, 2014 Nest building is impaired in the Ts65Dn
1008 mouse model of Down syndrome and rescued by blocking 5HT2a receptors. Neurobiol Learn
1009 Mem 116**:** 162-171.
1010 Herault, Y., J. M. Delabar, E. M. C. Fisher, V. L. J. Tybulewicz, E. Yu *et al.*, 2017 Rodent models in Down
1011 syndrome research: impact and future opportunities. Dis Model Mech 10**:** 1165-1186.
1012 Hoelter, S. M., C. Dalke, M. Kallnik, L. Becker, M. Horsch *et al.*, 2008 "Sighted C3H" mice - a tool for
1013 analysing the influence of vision on mouse behaviour? Frontiers in Bioscience 13**:** 5810-5823.
1014 Hughes, R. N., 2004 The value of spontaneous alternation behavior (SAB) as a test of retention in
1015 pharmacological investigations of memory. Neurosci Biobehav Rev 28**:** 497-505.
1016 Itohara, S., Y. Kobayashi and T. Nakashiba, 2015 Genetic factors underlying attention and impulsivity:
1017 mouse models of attention-deficit/hyperactivity disorder, pp. 46-51. Current Opinion in
1018 Behavioral Sciences.
1019 Kazuki, Y., F. J. Gao, Y. Li, A. J. Moyer, B. Devenney *et al.*, 2020 A non-mosaic transchromosomic mouse
1020 model of down syndrome carrying the long arm of human chromosome 21. Elife 9.
1021 Leal, S. L., and M. A. Yassa, 2015 Neurocognitive Aging and the Hippocampus across Species. Trends
1022 Neurosci 38**:** 800-812.
1023 Ling, K. H., C. A. Hewitt, K. L. Tan, P. S. Cheah, S. Vidyadaran *et al.*, 2014 Functional transcriptome
1024 analysis of the postnatal brain of the Ts1Cje mouse model for Down syndrome reveals global
1025 disruption of interferon-related molecular networks. BMC Genomics 15**:** 624.
1026 Lorenzi, H., N. Duvall, S. Cherry, R. Reeves and R. Roper, 2010 PCR prescreen for genotyping the Ts65Dn
1027 mouse model of Down syndrome. Biotechniques 48**:** 35-38.
1028 Luo, W., M. S. Friedman, K. Shedden, K. D. Hankenson and P. J. Woolf, 2009 GAGE: generally applicable
1029 gene set enrichment for pathway analysis. BMC Bioinformatics 10**:** 161.
1030 Marechal, D., V. Brault, A. Leon, D. Martin, P. L. Pereira *et al.*, 2019 Cbs overdosage is necessary and
1031 sufficient to induce cognitive phenotypes in mouse models of Down syndrome and interacts
1032 genetically with Dyrk1a. Hum Mol Genet.
1033 Martinez-Cue, C., C. Baamonde, M. Lumbreras, J. Paz, M. T. Davisson *et al.*, 2002 Differential effects of
1034 environmental enrichment on behavior and learning of male and female Ts65Dn mice, a model
1035 for Down syndrome. Behav Brain Res 134**:** 185-200.
1036 Matsumoto, S., S. Fujii, A. Sato, S. Ibuka, Y. Kagawa *et al.*, 2014 A combination of Wnt and growth factor
1037 signaling induces Arl4c expression to form epithelial tubular structures. EMBO J 33**:** 702-718.
1038 Moore, C. S., C. Hawkins, A. Franca, A. Lawler, B. Devenney *et al.*, 2010 Increased male reproductive
1039 success in Ts65Dn "Down syndrome" mice. Mamm Genome 21**:** 543-549.

Muñiz Moreno, M. D. M., V. Brault, M. C. Birling, G. Pavlovic and Y. Herault, 2020 Modeling Down syndrome in animals from the early stage to the 4.0 models and next. Prog Brain Res 251: 91-143.

Nakano-Kobayashi, A., T. Awaya, I. Kii, Y. Sumida, Y. Okuno *et al.*, 2017 Prenatal neurogenesis induction therapy normalizes brain structure and function in Down syndrome mice. Proc Natl Acad Sci U S A 114: 10268-10273.

Neumann, F., S. Gourdain, C. Albac, A. D. Dekker, L. C. Bui *et al.*, 2018 DYRK1A inhibition and cognitive rescue in a Down syndrome mouse model are induced by new fluoro-DANDY derivatives. Sci Rep 8: 2859.

Nguyen, T. L., A. Duchon, A. Manousopoulou, N. Loaëc, B. Villiers *et al.*, 2018 Correction of cognitive deficits in mouse models of Down syndrome by a pharmacological inhibitor of DYRK1A. Dis Model Mech 11.

O'Doherty, A., S. Ruf, C. Mulligan, V. Hildreth, M. L. Errington *et al.*, 2005 An aneuploid mouse strain carrying human chromosome 21 with Down syndrome phenotypes. Science 309: 2033-2037.

Olmos-Serrano, J. L., H. J. Kang, W. A. Tyler, J. C. Silbereis, F. Cheng *et al.*, 2016 Down Syndrome Developmental Brain Transcriptome Reveals Defective Oligodendrocyte Differentiation and Myelination. Neuron 89: 1208-1222.

Pizzo, L., M. Jensen, A. Polyak, J. A. Rosenfeld, K. Mannik *et al.*, 2019 Rare variants in the genetic background modulate cognitive and developmental phenotypes in individuals carrying disease-associated variants. Genetics in Medicine 21: 816-825.

Reeves, R. H., N. G. Irving, T. H. Moran, A. Wohn, C. Kitt *et al.*, 1995 A mouse model for Down syndrome exhibits learning and behaviour deficits. Nat Genet 11: 177-184.

Richtsmeier, J., L. Baxter and R. Reeves, 2000 Parallels of craniofacial maldevelopment in Down syndrome and Ts65Dn mice. Dev Dyn 217: 137-145.

Ruby, N., F. Fernandez, P. Zhang, J. Klima, H. Heller *et al.*, 2010 Circadian locomotor rhythms are normal in Ts65Dn "Down syndrome" mice and unaffected by pentylenetetrazole. J Biol Rhythms 25: 63-66.

Schultz, H., T. Sommer and J. Peters, 2015 The Role of the Human Entorhinal Cortex in a Representational Account of Memory. Front Hum Neurosci 9: 628.

Shaw, P. R., J. A. Klein, N. M. Aziz and T. F. Haydar, 2020 Longitudinal neuroanatomical and behavioral analyses show phenotypic drift and variability in the Ts65Dn mouse model of Down syndrome. Dis Model Mech 13.

Sierra, C., I. De Toma, L. L. Cascio, E. Vegas and M. Dierssen, 2021 Social Factors Influence Behavior in the Novel Object Recognition Task in a Mouse Model of Down Syndrome. Front Behav Neurosci 15: 772734.

Starbuck, J. M., T. Dutka, T. S. Ratliff, R. H. Reeves and J. T. Richtsmeier, 2014 Overlapping trisomies for human chromosome 21 orthologs produce similar effects on skull and brain morphology of Dp(16)1Yey and Ts65Dn mice. Am J Med Genet A 164A: 1981-1990.

Vorhees, C. V., and M. T. Williams, 2006 Morris water maze: procedures for assessing spatial and related forms of learning and memory. Nat Protoc 1: 848-858.

Yonemura, S., T. Matsui and S. Tsukita, 2002 Rho-dependent and -independent activation mechanisms of ezrin/radixin/moesin proteins: an essential role for polyphosphoinositides in vivo. J Cell Sci 115: 2569-2580.

1085

1086 **FIGURE LEGEND**

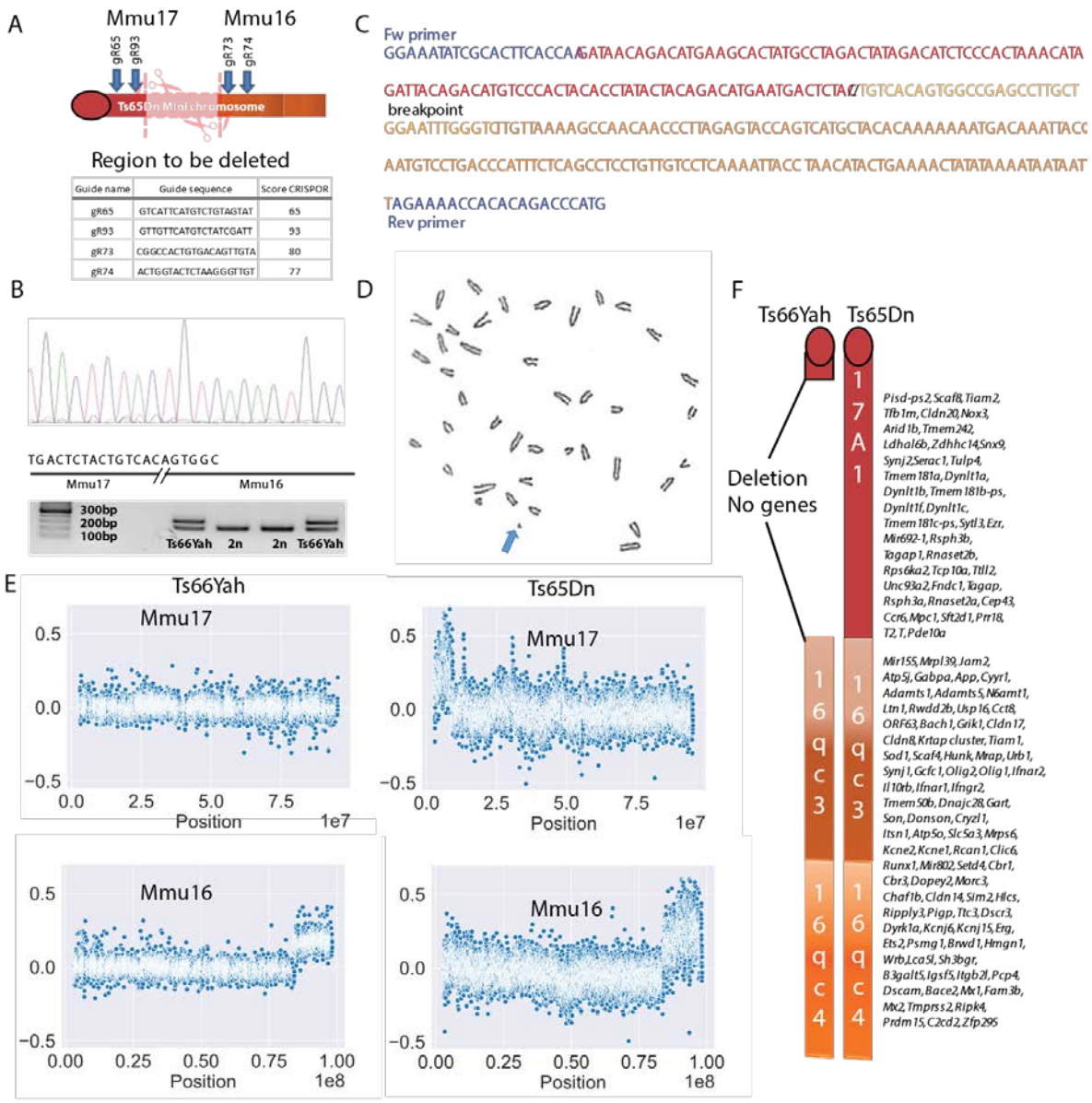

1087

1088 **Fig. 1. Generation and validation of the new Ts66Yah mouse model.**

1089 A. Schematic representation of the deletion produced in Ts65Dn using CrispR/Cas9 and two

1090 pairs of gRNA. B. Sequence electropherogram and PCR amplification products from the

1091 genotyping of Ts66Yah mice. C. Genomic sequence of the new junction found in the deleted

1092 minichromosome of Ts66Yah mice. D. Example of metaphase spread showing the presence of

1093 an additional minichromosome in Ts66Yah fibroblast. E. Comparative genomic hybridization

1094 (log2) of genomic DNA from Ts66Yah mice versus wild-type (AMADID 027411. Agilent

1095 Technologies 180K probes) compared to Ts65Dn mice (NimbleGen mouse HD2

1096 oligonucleotide arrays 2 100K probes). F. Schematic representation of the Ts66Yah and

1097 Ts65Dn minichromosomes.

1098

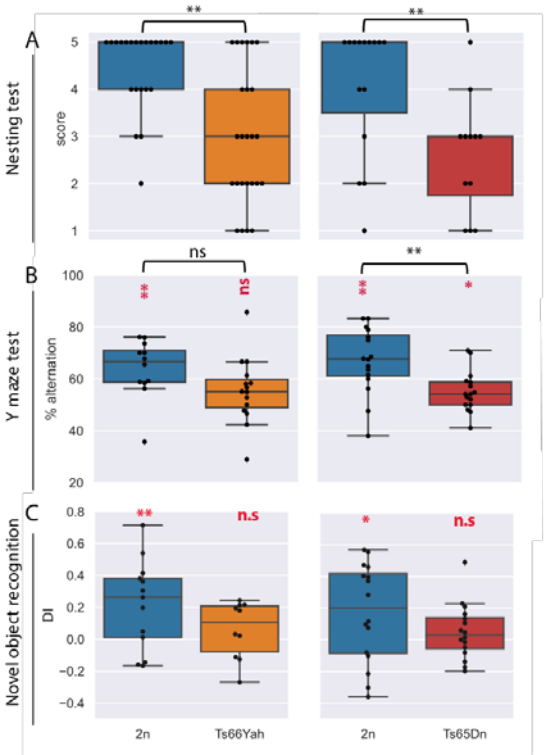

1099 **Fig. 2. Nesting activities and wroking memories display similar changes in Ts66Yah and**

1100 **Ts65Dn models.**

1101 A. Mice with trisomy showed deficits in building a nest (score below 3) while a majority of 2n

1102 mice were able to build a complete 3D nest (score above 3) (22 2n. 25 Ts66Yah and 15 2n. 12

1103 Ts65Dn). B. Although there was no significant difference int the percentage of alternation

1104 between 2n mice and Ts66Yah mice, level was significantly above 50% (chance level) only in

1105 2n and not inTs66Yah mice. Conversely, the Ts65Dn line showed a strong difference between

1106 genotypes, with a significant lower % of alteration for the trisomic group as compared to

1107 chance level, as well as a reduced spontaneous alternation as compared to 2n mice. C. In the
1108 NOR, the discrimination index analysis indicated that Ts66Yah and Ts65Dn mice were not able
1109 to distinguish the novel object (RI was close to 0). Overall, these tests indicated that working
1110 and episodic memories were similarly impaired in both DS mouse models, Ts66Yah and
1111 Ts65Dn. Box plots with the median and quartiles. * $p<0.05$. ** $p<0.01$. *** $p<0.001$. One
1112 sample T test result versus 0 was indicated in the graphic for RI.

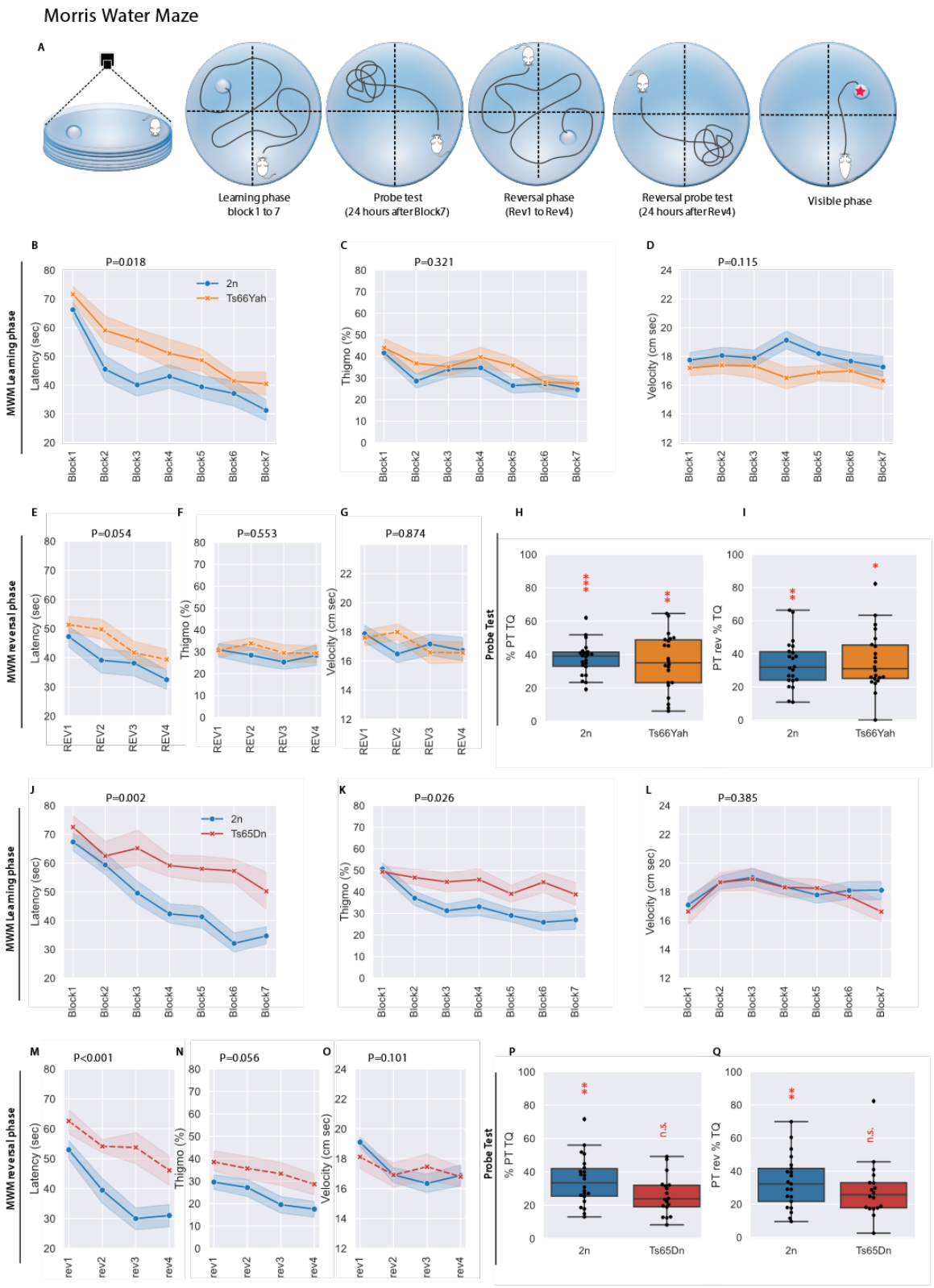

Fig. 3. Different effects on spatial learning and memory in the Morris water maze between Ts66Yah and Ts65Dn mice.

1116 A. Schematic representation of the test. B and J. Both trisomic mice (22 2n. 22 Ts66Yah and
1117 20 2n. 18 Ts65D) exhibited a delay in acquisition during the learning phase of the test, resulting
1118 in increased latency to find the PF. In addition, the Ts65Dn mice presented increased
1119 thigmotaxic behavior (C and K) while velocity was stable regardless of the genotype (D and L).
1120 In the probe test (H and P), only the Ts65Dn mice did not present increased exploration of the
1121 target quadrant, indicating a clear deficit in reference memory not observed in Ts66Yah mice.
1122 During the reversal phase, the augmented latency to find the OF was close to the significant
1123 level for the Ts66Yah mice (E), whereas the difference was clearly increased for the Ts65Dn
1124 mice. M. There was no difference in velocity (D,L and L,O) for both lines and the thigmotaxic
1125 behavior was not found in the Ts66Yah mice compared to Ts65Dn (C,F versus K,N). For the
1126 reversal probe test, once again only the Ts65Dn mice did not present preferences for the
1127 target quadrant (I.Q). The MWM result indicated a robust deficit in reference memory for the
1128 Ts65Dn mice which was not observed in Ts66Yah mice. Box plots with the median and
1129 quartiles * $p<0.05$. ** $p<0.01$. *** $p<0.001$. One sample T test result versus 25% is indicated in
1130 the graph for PT.

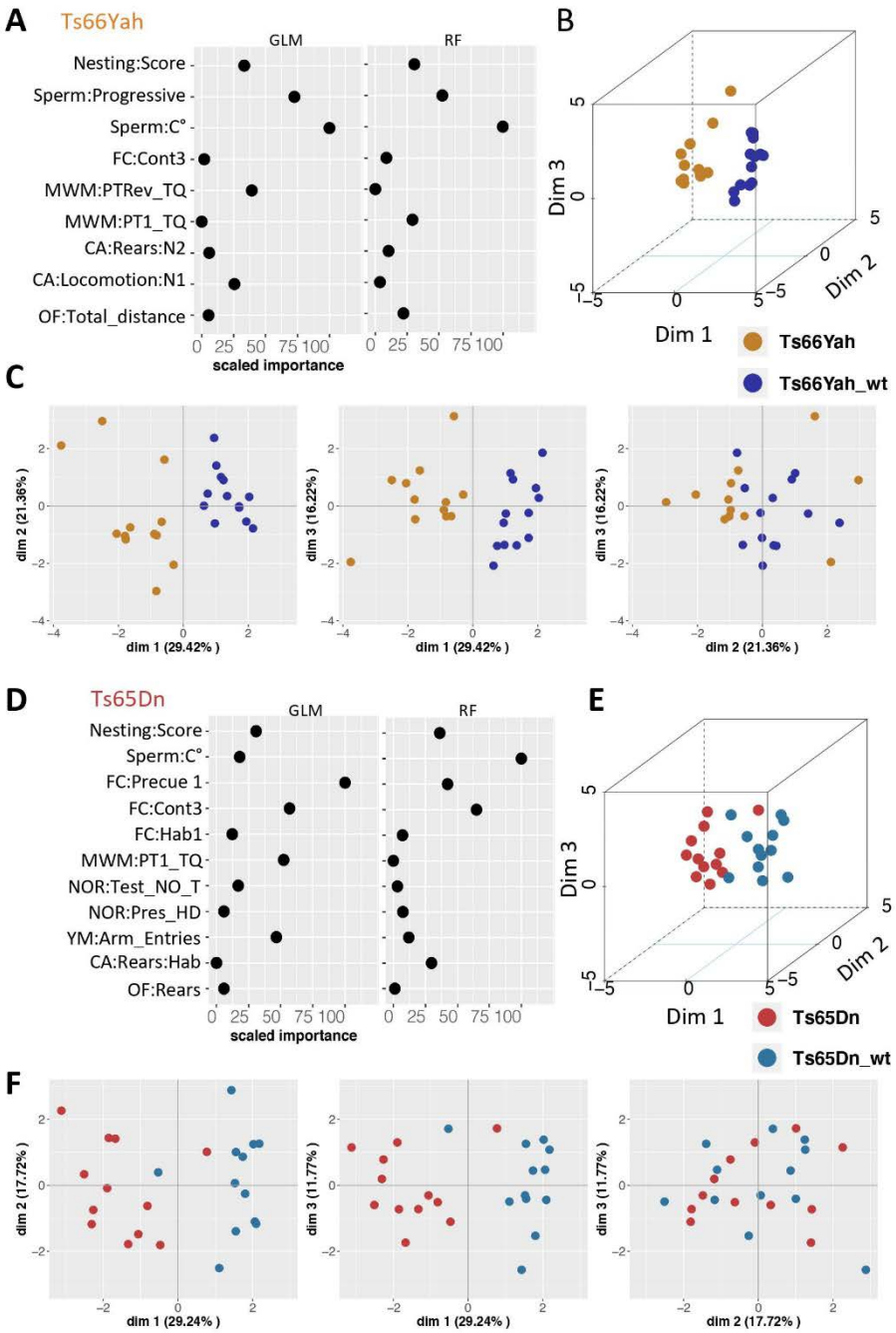

Fig 4: Identification of the strongest phenotypic variables contributing to the genotype discrimination in the Ts66Yah (A-C) and Ts65Dn (D-F) models. A-D. Importance of each explanatory phenotypic variable in the genotype discrimination. The explanatory variables selected were those known to contribute more than 30% to the genotype discrimination. These variables were identified using a principal component analysis (PCA) after applying a multi-factor analysis (MFA) of mixed data implemented using the MFAmix function from the

1138 PCAmixdata R package. The relevance of these variables to the genotype discrimination was
1139 analyzed using two different statistical classifiers: a Generalized Linear Model noted GLM and
1140 Random forest noted RF, both functions contained in the caret R package. All measures of
1141 importance are scaled to obtain a maximum value of 100 for the variable contributing most
1142 to the discrimination in the comparison of Ts66Yah DS mutants versus Wild-types. With GLM
1143 and RF we can identify the importance of each variable to discriminate each genotype. B-C.
1144 3D-PCA plots showing the individual animals clustering on the 3D space based on the PCA
1145 analyses performed with all the phenotypic variables and colored based on genotype and
1146 model as follows: in dark blue the Ts66Yah wild-types and in medallion yellow Ts66Yah DS
1147 mutants. C-F. Individual component map. The distribution in 2D space of the individual
1148 observation coordinates calculated based on the PCA analysis performed after the MFA
1149 implemented using the MFAmix function from the PCAmixdata R package.

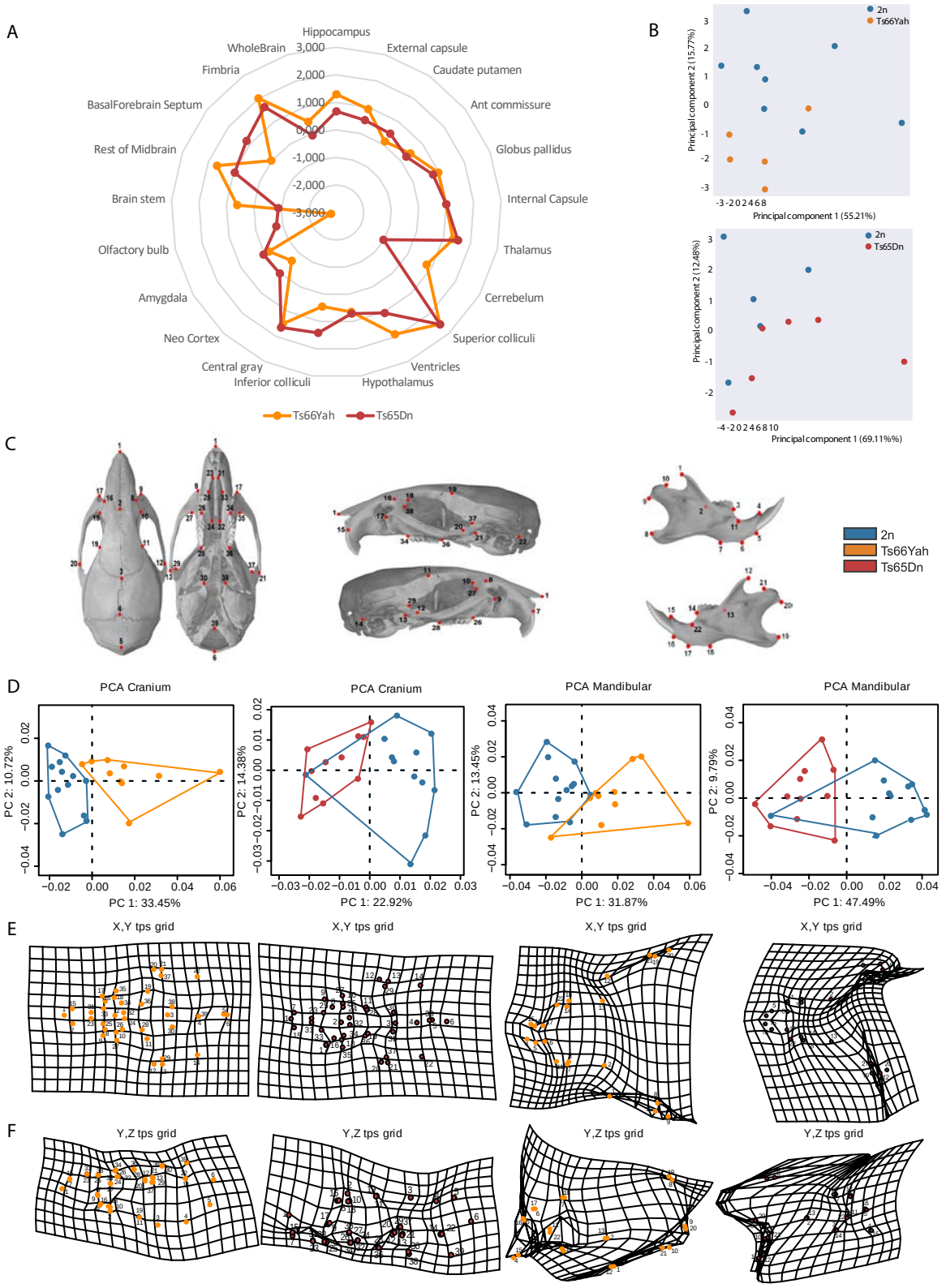

Fig. 5: Comparing morphological changes in the brain (MRI) and skull (CT scans) of the Ts66Yah and Ts65Dn. We analyzed different brain regions/structures taking into

consideration the whole brain volume. A. the Z-score was calculated as the mean of control (wt) mice minus the mean of transgenic mice divided by each type of wt and trisomic (Ts). Changes were similar between the Ts66Yah (2n: n=6. 7, Ts: n=7) and Ts65Dn (2n: n=5, Ts n=6) although the amplitude of the changes was less drastic in Ts66Yah than in Ts65Dn. B. PCA analysis indicated that Ts65Dn were more affected than their respective wt compared to the Ts66Yah line. C. The landmarks used for craniofacial analysis. D-F. Cranio-facial analysis. D. ACP analysis after generalized Procrustes indicated that for cranial skull and mandibular, the 2n group (n=13) and the Ts66Yah (n=10) group were well separated while the Ts65Dn (n=15) were less well separated from their control 2n littermates (n=16). E and F. the shape differences between the means of groups was visualized graphically by obtaining the average landmark coordinates for each group and the overall mean and plotting the differences as thin-plate spline transformation grids for the 2 axes. The XY axis was less affected than the YZ axis for both skull and mandible.

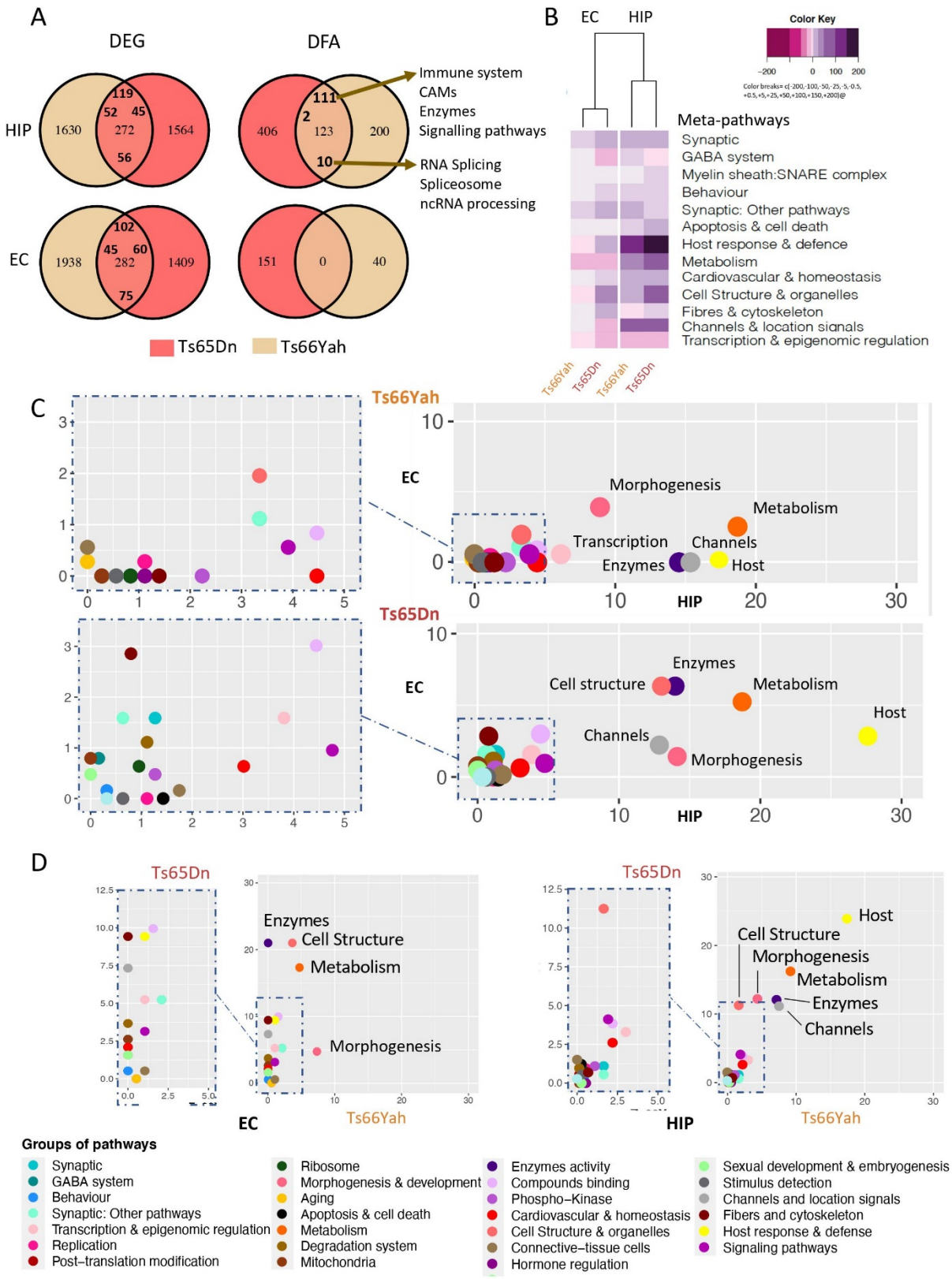
A
DEG
DFA
HIP
EC
1630
119
52
45
272
56
1564
406
111
2
123
10
200
1938
102
45
60
282
75
1409
151
0
40
Immune system
CAMs
Enzymes
Signalling pathways
RNA Splicing
Spliceosome
ncRNA processing
Ts65Dn
Ts66Yah
B
EC
HIP
Color Key
Meta-pathways
Synaptic
GABA system
Myelin sheath:SNARE complex
Behaviour
Synaptic: Other pathways
Apoptosis & cell death
Host response & defence
Metabolism
Cardiovascular & homeostasis
Cell Structure & organelles
Fibres & cytoskeleton
Channels & location signals
Transcription & epigenomic regulation
Ts66Yah
Ts65Dn
Ts66Yah
Ts65Dn
C
Ts66Yah
EC
Morphogenesis
Metabolism
Transcription
Channels
Enzymes
Host
HIP
Ts65Dn
EC
Enzymes
Cell structure
Metabolism
Host
Channels
Morphogenesis
HIP
D
Ts65Dn
Enzymes
Cell Structure
Metabolism
Morphogenesis
EC
Ts66Yah
Ts65Dn
Host
Cell Structure
Morphogenesis
Metabolism
Enzymes
Channels
HIP
Ts66Yah
Groups of pathways
Synaptic
GABA system
Behaviour
Synaptic: Other pathways
Transcription & epigenomic regulation
Replication
Post–translation modification
Ribosome
Morphogenesis & development
Aging
Apoptosis & cell death
Metabolism
Degradation system
Mitochondria
Enzymes activity
Compounds binding
Phospho–Kinase
Cardiovascular & homeostasis
Cell Structure & organelles
Connective–tissue cells
Hormone regulation
Sexual development & embryogenesis
Stimulus detection
Channels and location signals
Fibers and cytoskeleton
Host response & defense
Signaling pathways

1166

1167 **Fig. 6. Functional analysis of expressed genes and pathways altered in DS model Ts66Yah**
1168 **compared to DS model Ts65Dn.** A. Venn diagrams showing in the left panel the DEGs found
1169 in common between the Ts66Yah and Ts65Dn hippocampi (HIP) in the upper part and the
1170 entorhinal cortex (EC) in the lower one. The shared DEGs correspond to 14%, 14%, 12% and
1171 16% of the total DEGs identified for the Ts66Yah HIP, Ts65Dn HIP, Ts66Yah EC and the Ts65Dn
1172 EC , respectively. Right panel highlighting the model specific and common pathways altered
1173 between Ts66Yah and Ts65Dn HIP samples in the upper part and the EC datasets of both the
1174 Ts65Dn and Ts66Yah models in the lower part. The percentage of shared pathways reached
1175 23% and 38% of the total altered pathways in Ts65Dn hippocampi compared to Ts66Yah
1176 hippocampi and none were found in common between the models for the EC region**.** B**.**
1177 Heatmap representation of the number and regulation sense of the meta-pathways found in
1178 the Ts65Dn and Ts66Yah HIPand EC. The color key breaks represent the number of pathways
1179 within the meta-pathways. The minus or pink color represent down regulated pathways, the
1180 white color indicates that no pathway was found in the meta-pathway and the purple or
1181 positive numbers stand for up regulated pathways respectively. C. Scatter-plot showing the
1182 inter-tissue comparison of the percentage of pathways included on each meta-pathway
1183 (group of pathways) normalized by the total number of unique pathways per meta-pathway
1184 for Ts66Yah (upper panel) and the Ts65Dn (lower panel) on the x-axis and y-axis representing
1185 the HIP and the EC for the Ts66Yah or Ts65Dn models, respectively. D. Similar representation
1186 showing the inter-model comparison with the percentage of pathways included on each meta-
1187 pathway (group of pathways) normalized by the total number of unique pathways per meta-
1188 pathway found in the HIP of Ts66Yah (x-axis) in comparison with Ts65Dn (y-axis).
1189

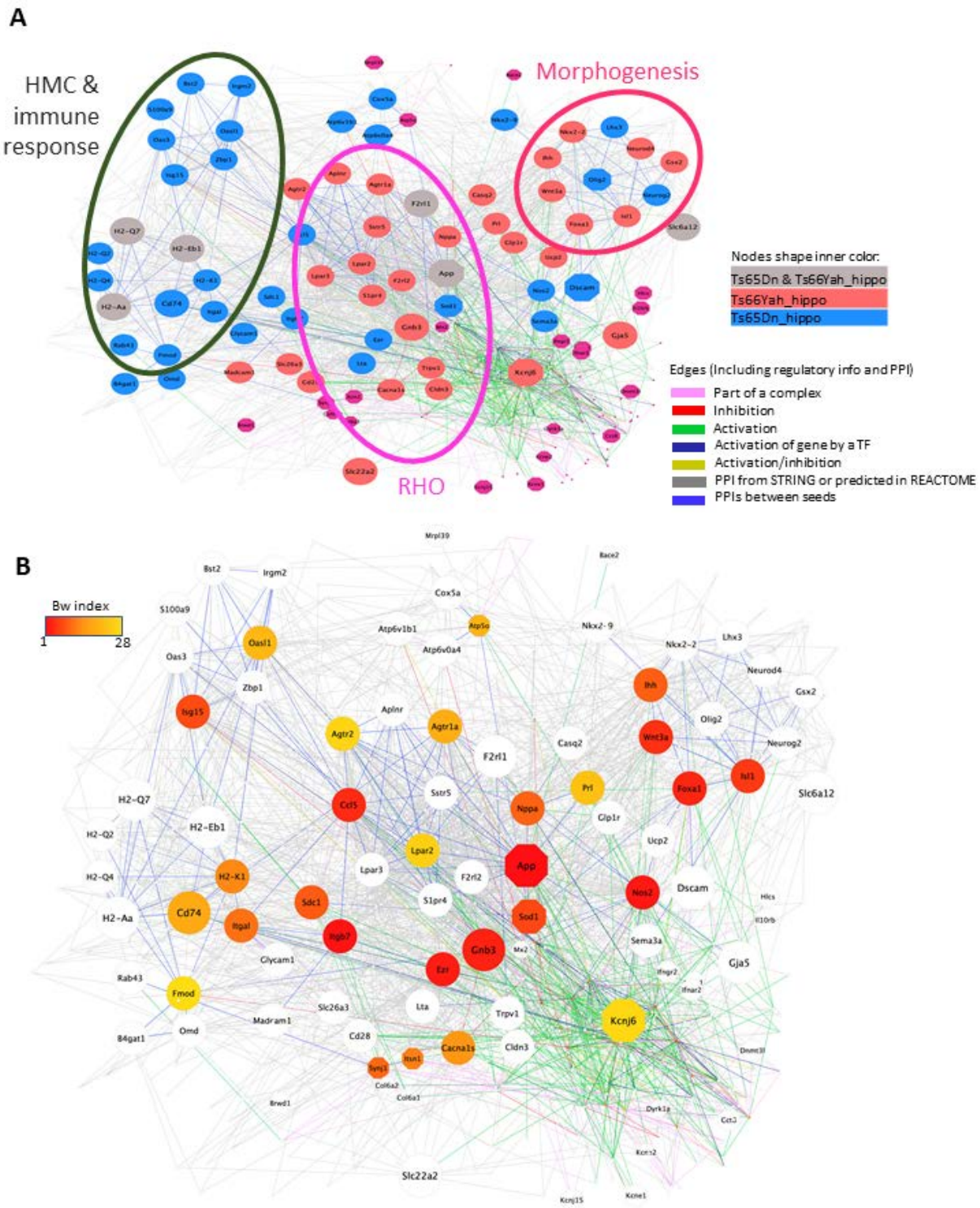

1190

1191 **Fig. 7. Central Protein-protein interaction and regulatory gene connectivity network**

1192 **(RegPPINets) involved in the synaptic meta-pathway identified in Ts65Dn and Ts66Yah,**

1193 **highlighting the top 30 genes identified by betweenness centrality analysis.** The central

1194 networks (A and B) were extracted from RegPPINet. These networks were built by querying

1195 STRING for all the DEGs identified by gage as contributing to brain synaptic alteration and
1196 selecting the PPIs with a medium confidence score (CS), CS = 0.4 from all sources of evidence.
1197 Then, the network was further annotated with regulatory information using REACTOME (See
1198 Supplementary Materials and Methods). A. Central RegPPINets of genes involved in the
1199 synaptic meta-pathway identified in Ts65Dn and Ts66Yah, highlighting the main subnetworks
1200 found. B. The same central RegPPINets highlighting in color from red to yellow the proteins
1201 more central for the communication flow over the network identified by the centrality analysis
1202 using the betweenness index.
1203
1204 **TABLES**
1205

Genetic Background	Time / event	Transmission rate	Nb of individuals
B6C3B	Nov-Dec 2017	53%	30
	Jan-Apr 2018	52%	119
	Aug-Dec 2018	32%	112
B6J	1st backcross	56%	61
	2nd backcross	29%	17
	3rd backcross	35%	17
	4th backcross	24%	21

1206
1207
1208
1209
1210
1211 **Table 1: Transmission of the Ts66Yah minichromosome in the B6C3B and B6J genetic**
1212 **backgrounds**
1213
1214
1215

	Ts65Dn		Ts66Yah	
Variable	2n	DS	2n	DS
GLMNET				
Sperm:Progressive	17.6	27.5	15.7	15.7
FC:Hab2	10.1	19.1	18.0	10.1
MWM:PTRev_TQ	5.2	22.4	8.4	5.2
NOR:Test_NO_%	12.1	25.9	12.3	12.1
NOR:Test_NO_T	0.3	19.1	12.5	0.3
YM:Spont_Alter	8.1	17.6	7.1	7.1
CA:Rears:N2	25.1	29.0	50.0	25.1
CA:Locomotion:Light	3.6	2.4	3.5	2.4
CA:Locomotion:Hab	0.0	0.0	11.2	23.7
OF:Sterotypies	22.1	21.7	21.7	100.0
OF:Rears	6.4	40.8	15.4	6.4
Random Forest				
Sperm:Progressive	30.3	58.2	39.6	18.0
FC:Hab2	50.0	13.9	13.4	19.5
MWM:PTRev_TQ	10.9	29.7	13.9	6.9
NOR:Test_NO_%	11.6	16.6	29.6	25.1
NOR:Test_NO_T	48.4	15.1	12.6	41.5
YM:Spont_Alter	34.0	31.1	15.5	21.9
CA:Rears:N2	27.9	72.4	25.3	13.6
CA:Locomotion:Light	24.4	14.0	8.5	21.0
CA:Locomotion:Hab	21.5	33.3	1.5	6.6
OF:Sterotypies	75.7	47.3	0.0	100.0
OF:Rears	18.5	5.3	15.4	5.1

Table 2. Discriminating variables identified from the GLM-Net and RF analysis combining the Ts66Yah &Ts65Dn data.

	Ts65Dn EC	Ts65Dn HC	Ts66Yah EC	Ts66Yah HC
Differentially Expressed Genes (DEGs) identified by FCROS	1691	1836	2220	1902
Genes from the Mmu17 centromeric genes				
Expressed genes	53	53	53	53
Upregulated Trisomic (TEGs)	41	37	7	10
Genes from the Mmu16 homologous region to Hsa21				
Expressed genes	94	94	94	94
Upregulated Trisomic (TEGs)	81	85	82	84
Number of GAGE KEGG and GOs (CC.BP.MF) terms dis-regulated in the trisomic models (FDR<0.1)	135	493	40	323
Number of GAGE KEGG and GOs upregulated in the trisomic models (FDR<0.1)	95	459	1	260

1239

1240 **Table 3: Summary of the differential expression analysis and differential functional analysis**

1241 **for each DS model dataset**.

1242